Summer 2017

Electronic Structure Evaluation of Competing Pathways in the Gold(III)-Catalyzed Ohloff-Rautenstrauch Cyclosimerization Converting Propargylic Acetates to Carene-like Natural Products

Jeremy M. Hines
Missouri State University, Hines057@live.missouristate.edu

ELECTRONIC STRUCTURE EVALUATION OF COMPETING PATHWAYS IN THE GOLD(III)-CATALYZED OHLOFF-RAUTENSTRAUCH CYCLOSIMERIZATION CONVERTING PROPARGYLIC ACETATES TO CARENE-LIKE NATURAL PRODUCTS

A Master's Thesis

Presented to

The Graduate College of

Missouri State University

In Partial Fulfillment

Of the Requirements for the Degree

Master of Science, Chemistry

By

Jeremy Hines

August 2017

ELECTRONIC STRUCTURE EVALUATION OF COMPETING PATHWAYS IN THE GOLD(III)-CATALYZED OHLOFF-RAUTENSTRAUCH CYCLOSIMERIZATION CONVERTING PROPARGYLIC ACETATES TO CARENE-LIKE NATURAL PRODUCTS

Chemistry

Missouri State University, August 2017

Master of Science

Jeremy Hines

ABSTRACT

Propargylic acetates can lead to complex transformations upon exposure to a gold catalyst. Gold catalyzed transformations also allow for simple synthesis of a number of natural products. Gold (III)-cycloisomerization of a 5-acetoxy-1,6-enyne is reported to proceed through two pathways that differ in the order of major events: cyclization followed by ester migration ("cyclization first") or the reverse ("migration first"). Both pathways could theoretically proceed in either order. This rearrangement is called the Ohloff-Rautenstrauch rearrangement and has high regio- and stereocontrol affording a bicylo[4.1.0]heptane carbon substructure. This rearrangement allows for the synthesis of the carene class of natural products. Computational modeling determining the mechanism and preference for the pathways in the gas- and solvent-phase (dichloroethane, IEFPCM) are described herein. Structures for the pathways are found using the B2PLYP/6-31G(d)-LANL2DZ model chemistry while energies are found at the B2PLYP-D3/def2TZVP//B2PLYP/6-31G(d)-LANL2DZ level. Both pathways feature multiple steps with low energy barriers. Highest-energy structures for both pathways are close in energy ($\Delta\Delta E^{\ddagger}$ = 2.8 kcal/mol for solvent phase). Turnover frequency for each pathway are calculated suggesting that the cyclization first pathway may dominate.

KEYWORDS: DFT, gold (III), propargylic acetate, carene, natural products

This abstract is approved as to form and content

_____

Matthew R. Siebert, PhD
Chairperson, Advisory Committee
Missouri State University

ELECTRONIC STRUCTURE EVALUATION OF COMPETING PATHWAYS IN THE GOLD(III)-CATALYZED OHLOFF-RAUTENSTRAUCH CYCLOSIMERIZATION CONVERTING PROPARGYLIC ACETATES TO CARENE-LIKE NATURAL PRODUCTS

By

Jeremy Hines

A Masters Thesis
Submitted to the Graduate College
Of Missouri State University
In Partial Fulfillment of the Requirements
For the Degree of Master of Science

August 2017

Approved:

_____
Matthew R. Siebert, PhD.

_____
Gary A Meints, PhD.

_____
Maria Stepanova, PhD.

_____
Gautam Bhattacharyya, PhD.

_____
Julie Masterson, PhD: Dean, Graduate College

ACKNOWLEDGEMENTS

I dedicate this thesis to my parents for their endless support and encouragement.

TABLE OF CONTENTS

LIST OF TABLES

LIST OF FIGURES

GOLD REACTIVITY

Gold, known as “the king of metals”, has been prized throughout human history. This metal was so sought after for its unique golden color and its seemingly never-diminishing shine. Being very malleable it is easily shaped into works of art coveted by kings and the wealthy. Stores of gold would be locked away as proof of wealth and to be later used as currency.[1] But why is this metal so desired even though it seemingly had no practical uses in history? This may be due to the chemical properties of gold metal. From just looking at the golden color it is easy to tell apart from other metals. The next noticeable property is that gold is chemically inert hence it is considered a “noble metal”. Being resistant to oxidation under normal conditions, it is able to be mined, shaped and for centuries will retain its radiance.[1] Despite this observed inertness it will be dissolved in aqua regia or in solutions containing cyanide salts, which allows gold to be extracted from ores.

Gold properties

What gives gold these interesting properties, such as its golden color and resistance to oxidation under normal conditions, compared to similar metals, like silver or copper? As you move down the periodic table, nuclear charge increases, and electrons begin to show increased speed. By application of Einstein’s theory of special relativity, the mass of these quickly moving electrons will increase compared to the mass of a resting electron. (Equation 1)

$$m = m_o [1 - (v/c)^2]^{-1/2}$$

Equation 1. Equation for relativistic mass. m is the relativistic mass at a velocity (v). m_o is the mass of the object at rest. Speed of light (c). At high v the (v/c) becomes larger (closer to 1) raising the mass of the object.

This increased mass of electrons affects both the energy and the size of the orbitals.[2] The direct result of this is the contraction of the *s* orbitals and to a lesser extent *p* orbitals. These electrons are now more strongly bound and shield the nuclear charge. The *d* and *f* orbitals are not as strongly affected by these effects, but are indirectly affected due to the increased shielding from the nucleus so they expand. Though these effects are present in all atoms, they are not significant in elements in the first three rows of the periodic table. However, for heavy atoms, such as gold to bismuth, these effects are on the order of bond energies. This effect now can have serious impact on calculations involving these atoms with high nuclear charge.

These effects are the reasons for the unique properties of gold. The contraction of the 6*s* orbital increases the first ionization potential of gold to a level higher than silver. Gold requires a stronger reagent to oxidize it than silver, which will tarnish in air over time.[3] With the expansion of the 5*d* orbital in gold these electrons are more accessible and making the +3 oxidation state more easily obtained (silver doesn't commonly reach this oxidation). The color of gold can also be explained by these effects, where absorption energy is adjusted for the transition of the 5*d* band, (now higher in energy), and the now lowered in energy 6*s* band.[4]

These gold species are highly electrophilic, and are highly selective to activating a variety of π-systems. Early reports of homogenous gold catalysis were seen in 1986 in the

work by Ito and Hayashi[5]. The pair reported use of a chiral gold (I) catalyst to form an oxazoline from the addition of an isocynate onto an aldehyde (Figure 1).

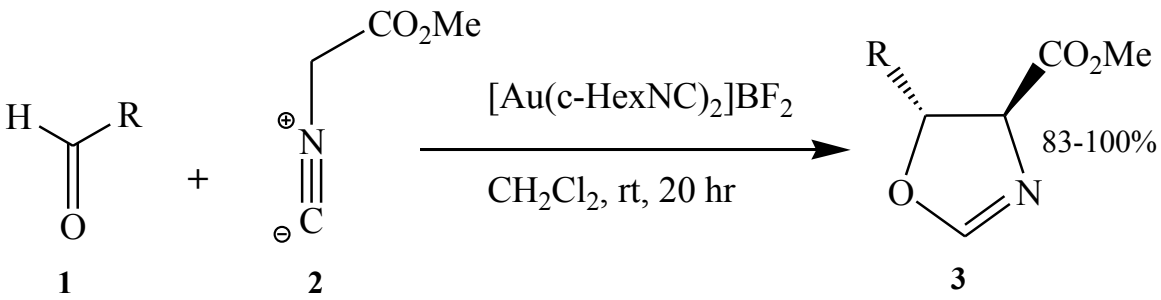

Figure 1 Synthesis of oxazoline (**3**) by addition of isocyanate (**2**) onto an aldehyde (**1**) by use of chiral Gold (I) catalyst.

Both gold (I) and (III) are effective at activating carbon-carbon multiple bonds (alkenes, alkynes, allenes); gold (III) can also activate carbonyl groups (aldehydes and ketones). Upon coordination by a gold catalyst these π-systems are now activated towards nucleophilic attack. Nucleophiles of the carbon, oxygen, nitrogen and sulfur species have proven to be effective in the these types of catalyzed reactions.[4]

Alkene Activation. The coordination of the metal to the π-systems is the first step in these catalytic processes. The binding to alkenes is described by the Dewar-Chat-Duncanson[6,7] model. This model involves a combination of π-electron donation and metal back-bonding. An alkene, in the simplest case ethylene, donates π-electrons to the empty *d*-orbital of the gold (Figure 2 top). This explains a T-shape geometry in the metal complex. Additionally, gold participates in back donation using a different *d*-orbital into the anti-bonding (π*) orbital of the ethylene forming a metallacyclopropane ring structure. Both of these effects weaken the π-bond, lengthening the carbon-carbon distance.[4]

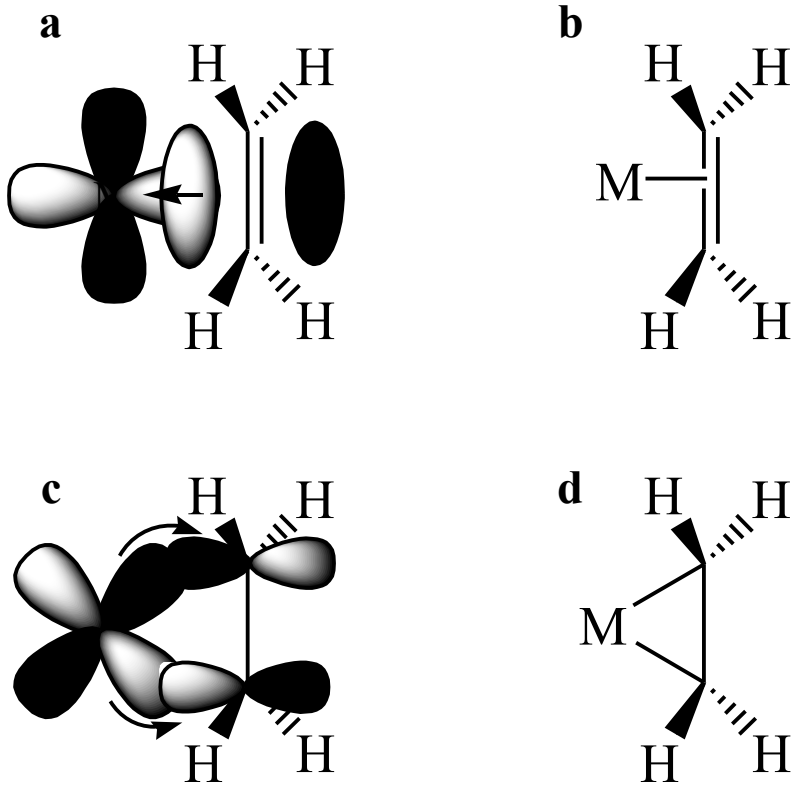

Figure 2. Orbital interactions of metal-ethylene bonding: (a) π-orbital of ethylene donating electrons to empty d-orbital of the metal. (c) Metal back bonding of the filled *d*-orbital to the anti-bonding π* orbital of the ethylene. Limiting structures of the metal-ethylene complex: (b) T-shaped structure. (d) Metallacyclopropane.

Alkyne Activation. Binding to carbon-carbon triple bonds adds an extra π-bond into the picture that the metal can interact with. The alkyne consists of two orthogonal π-bonds. The major interaction of the metal-alkyne, in this example acetylene, is the π-bond donating to the appropriate empty *d*-orbital, followed by the back bonding of a filled *d*-orbital that is in the plane of the anti-bonding π* of the alkyne. These two interactions are similar to the metal-alkene interaction specified before. The orthogonal anti-bonding π*-bond can accept electrons from the parallel *d*-orbital of the metal, while the bonding π-bond can donate to the perpendicular *d*-orbital. These interactions are very small due to

the limited overlap of these orbitals (these interactions are shown in Figure 3). The gold forms an η^2-complex with the π-bond for symmetric molecules.[4]

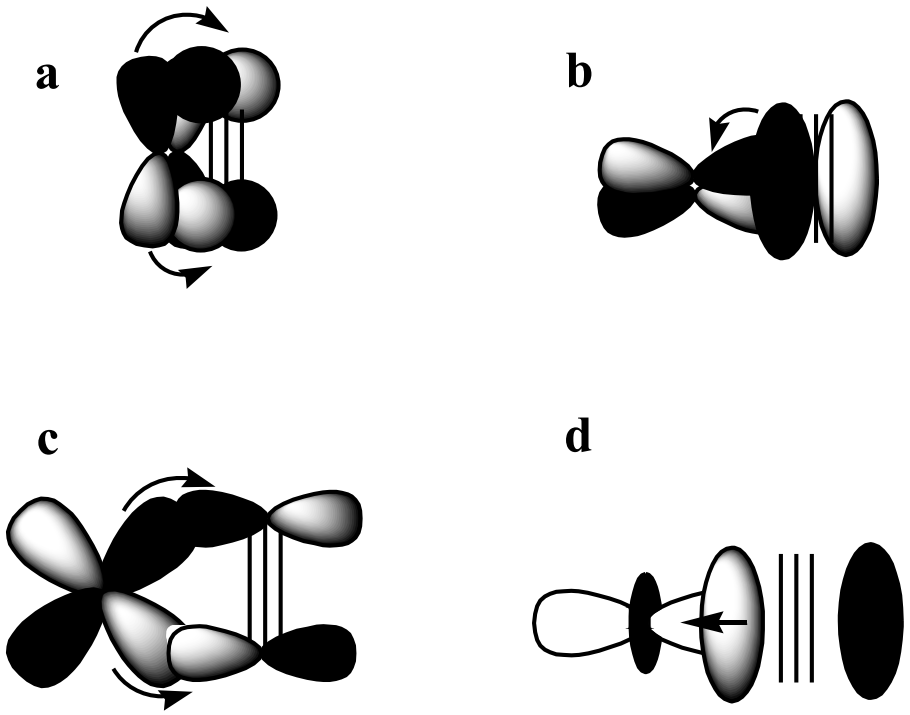

Figure 3. Orbital diagrams showing metal – acetylene interaction (a) parallel d_{xy} orbital donates electrons to orthogonal antibonding π*-orbital. (b) perpendicular d_{yz} orbital accepts electrons from orthogonal π-orbital. (c) d_{xz} orbital in the plane of the alkyne donates electrons to the antibonding π* orbital. (d) empty d_z^2 orbital accepts electrons from the bonding π-orbital

In all the cases the coordination of the metal increases the electrophilic nature of the π-system. Structurally, the π-bond weakens from this coordination. These interactions deform the carbon atoms towards tetrahedral (from trigonal planer) and bent (from linear) for the complexed alkene and alkyne, respectively. After coordination with gold, the activated π-system is prone to addition of a nucleophile. Nucleophilic attack at one of the carbon ends causes the gold to slip towards the other end of the π-system. Upon the

addition of the nucleophile the catalyst can be regenerated addition of a hydrogen. A simple scheme is shown in Figure 4 involving the nucleophilic addition to acetylene.[4]

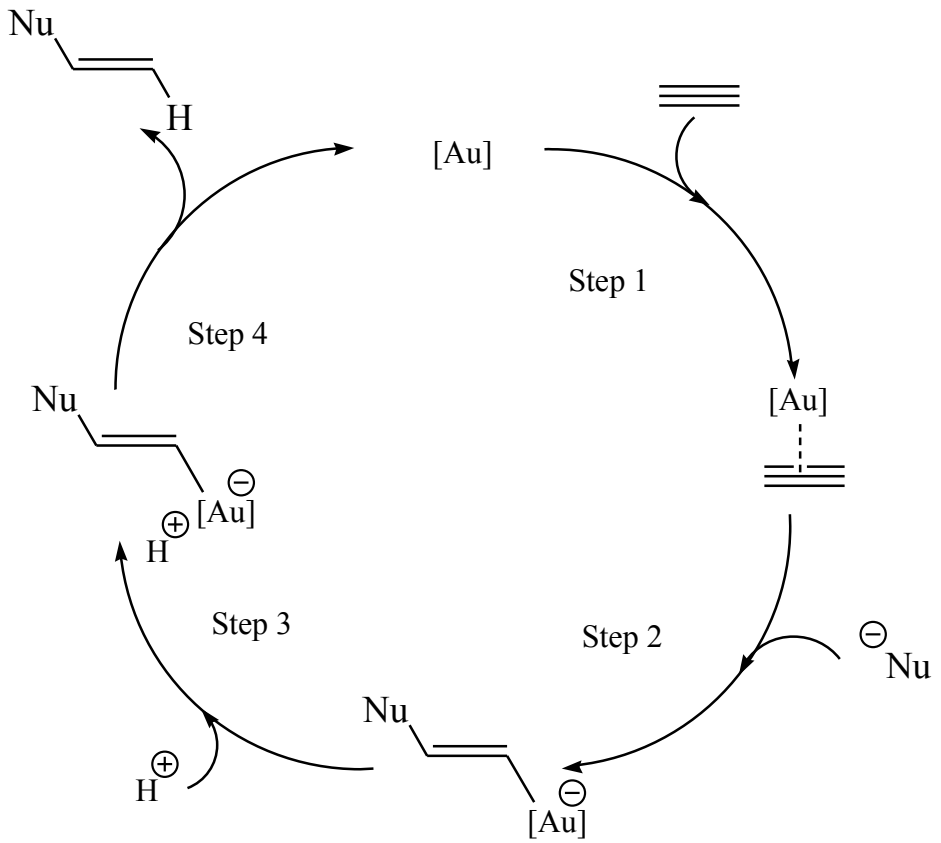

Figure 4. Nucleophilic addition onto acetylene. Step 1: electrophilic activation of acetylene of the gold. Step 2: nucleophilic attack onto the acetylene. Step 3: reductive elimination and regeneration of the catalyst

An additional result of the expansion of the 5*d* orbital (due to relativistic effects) is the ability of the electrons to act as a Lewis base to help stabilize carbocationic intermediates. This can provide interesting rearrangements that create more complex structures. A simple example would be the nucleophilic attack of an alkene onto a coordinated alkyne, where this forms a cyclopropane ring structure (Figure 5).

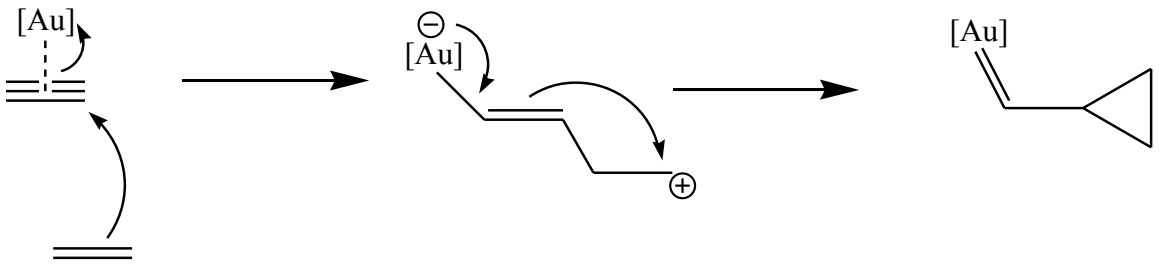

Figure 5. A coordinated alkyne undergoes attack by an alkene forming a carbocation, which rearranged to be stabilized by donation of electrons from catalyst.

Alkynes can be activated to the attack of both carbon and heteroatoms, this leads to a wide range of structures that can be formed. That range from simple nucleophilic additions of alkynes to cyclodimerizations forming complex ring structures.[4]

Reactions of Gold and Alkynes

An interesting and practically useful property of gold is its low oxyphilicity. Even in the presence of oxygen containing functional groups and water, gold is able to selectively activate π-systems. Teles and Tanaka even explored the addition of water and alcohols onto alkynes . The hydration of alkynes was shown to be an improvement on previous methods, tend to use toxic Hg (II) salts under highly acidic conditions. These studies highlighted the impact of gold catalysis in organic synthesis with the activation of alkynes allowing for easily accessible molecular complexity.

Oxygen Nucleophiles. Teles[8] and Tanaka[9] used AuMe(L) (L=phosphine, phosphite or arsine) to hydrate alkynes efficiently, in a Markovnikov-fashion on a variety of alkyne substrates (both terminal and internal; Figure 6). One limitation to this

methodology is that there is still a need for highly acidic solutions preventing the hydration of substrates with acid-labile groups.

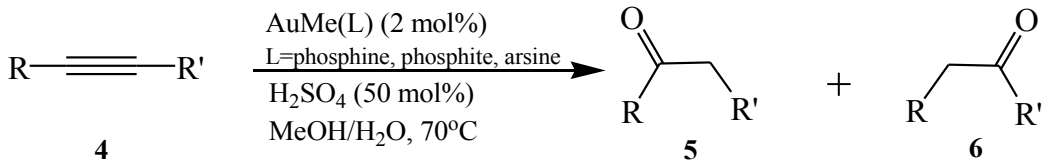

4 **5** **6**

Figure 6. Hydration of an alkyne (**4**) by a gold (I) catalyst that forms ketones, **5** and **6.** This reaction requires highly acidic conditions in methanol and water.

Leyva and Corma[10] using the gold (I) catalyst AuSPhosNTf$_2$ in methanol, found that an acid is no longer required and that the reaction can be carried out at room temperature when hydrating 3-butyn-2-ol (Figure 7, 96% yield). Additionally they state that the type of ligand on the catalyst dramatically effects the reactivity.

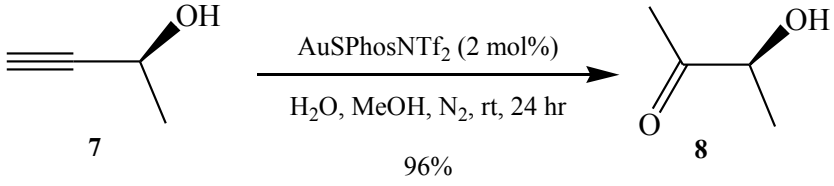

7 **8**

Figure 7. Hydration of 3-butyn-2-ol (**7**) by AuSPhosNTf$_2$. Conditions are milder than reaction found in Figure 6 because acidic conditions are not needed at can be run at room temperature.

Utimoto[11] reported the use of gold (III) chloride-catalyzed addition of methanol onto a range of alkynes both terminal and internal, to provide dimethyl acetals (Figure 8).

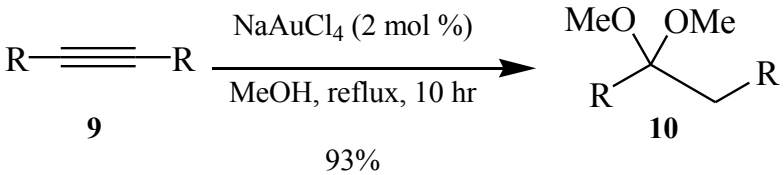

9 **10**

Figure 8. Hydroalkoxylation of alkyne **9** forming dimethyl acetal **10** by gold (III) catalyst in methanol.

These reports showed effective intermolecular nucleophilic addition to alkynes but intramolecular addition by a tethered functional group can occur. Many oxygen containing functional groups may act as a nucleophile, however in this context, the most common alcohols and ketones. A few examples of these types of reactions are found in the synthesis of furans by gold (I) catalyzed reactions with alkynediols (**11**),[12] alkynones (**12**),[13] and even alkynyloxiranes (**13**)[14] (Figure 9).

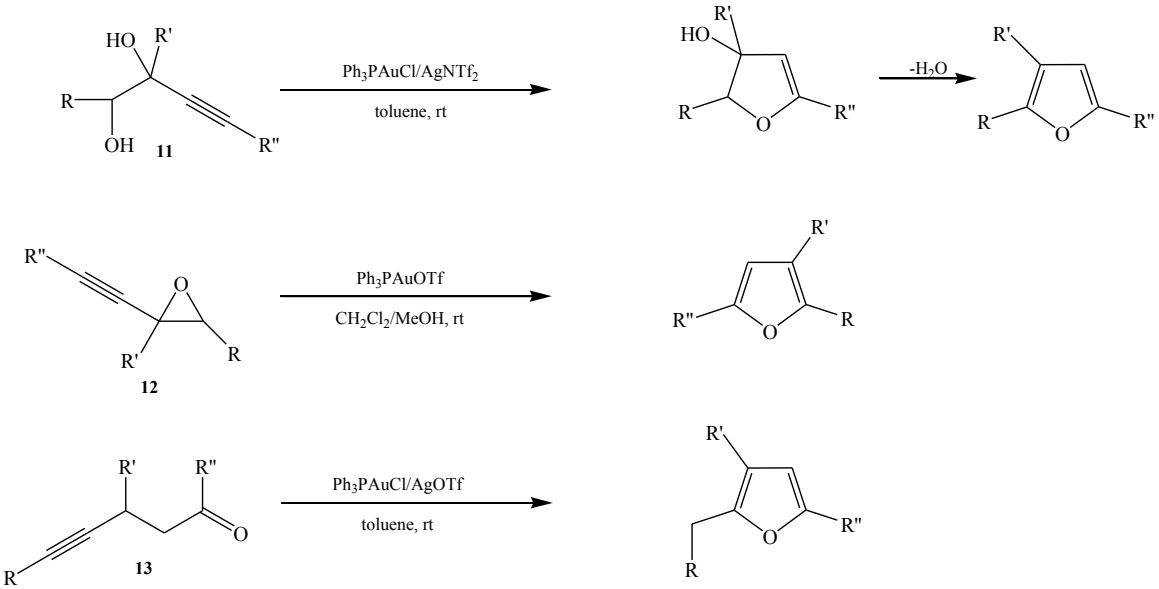

Figure 9. Formation of furans by nucleophilic at of tethered oxygen nucleophiles, alkynediols, alkynones, and alkynyloxiranes.

Carbon Nucleophiles. Addition of carbon nucleophiles leads to the formation of new carbon-carbon bonds. Examples include additions of alkenes onto alkynes or even aromatic rings onto alkynes. Additions of alkenes onto alkynes form a cyclobutenes (Figure 10). Moderate yields are observed often, some loss of yield attributed to the fact

that either a reactant can act as a substrate for the gold catalyst leading to competition in the reaction.

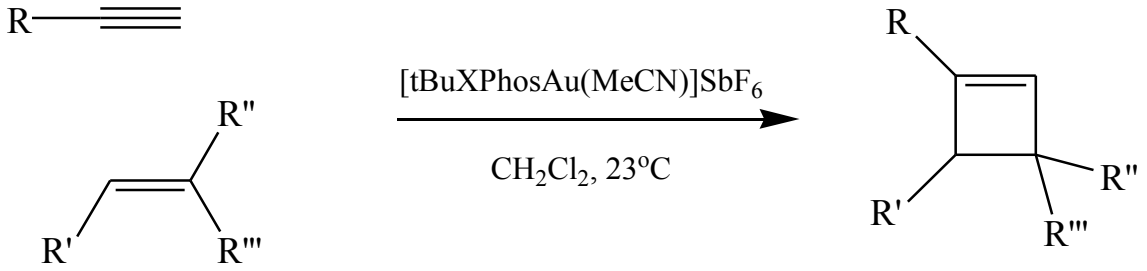

Figure 10. Formation of a cyclobutene by the nucleophilic attack of alkene onto terminal alkyne in 1,2-dichloroethane.

One of the most studied gold-catalyzed reactions involving formation of carbon-carbon bonds are 1,*n*-enynes. Rearrangements of 1,*n*-enynes allows access to complex structures from simple reactants. While other transition metals have been used in cyclization of enynes, gold is the most effective. These gold-catalyzed reactions take place under milder conditions.[4] 1,6-enynes are one of the more readily studied substrates in gold catalysis. These reactions can lead to different skeletal rearrangements via 5-*exo*-dig or 6-*endo*-dig pathways (Figure 11).

In the 5-*exo*-dig pathways cyclizations forming dienes are the major products. The first set of dienes (**a**) are formed from single cleavage rearrangements where a 1,3 migration of the terminal carbon of the alkene moves to the terminal end of the alkyne. The formation of dienes **b** can be explained by a double cleaved rearrangement involving the insertion of the terminal carbon of the alkene between the carbons of the alkyne. Formation of diene **c** is done by 1,6-enynes containing terminal alkenes and/or tethered with heteroatoms to provide the six-membered rings containing a diene.[4] 1,6-enynes

tethered by an ether or sulfonamide rearrange by the 6-*endo*-dig pathway forming oxa- or aza-bicylo[4.1.0]hept-4-enes (**d**).

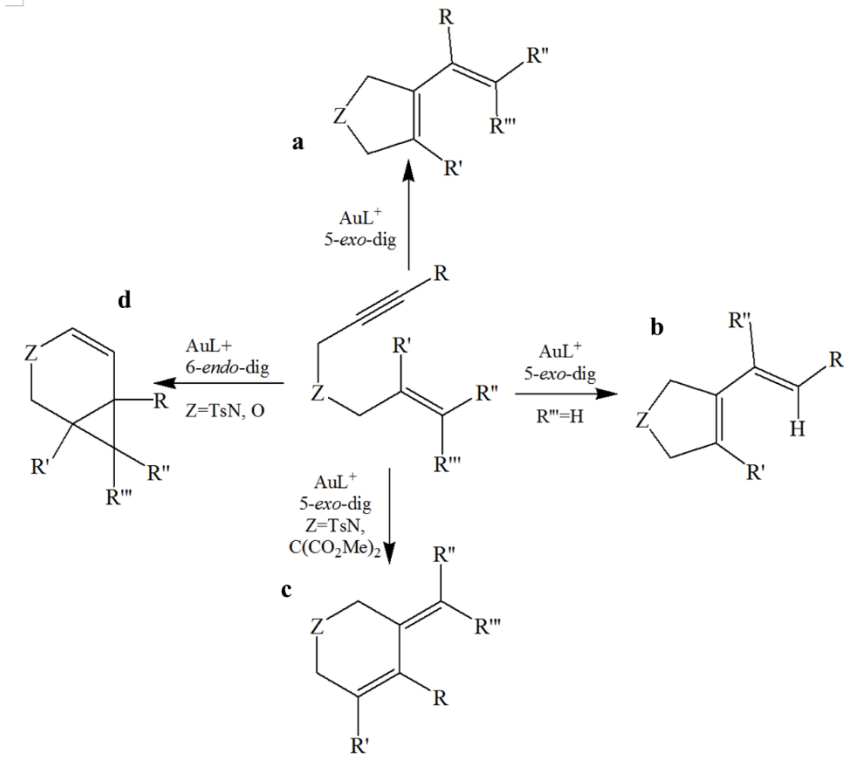

Figure 11. Gold-catalyzed rearrangement of 1,6-enynes by either 5-*exo*-dig or 6-*endo*-dig pathways. 5-*exo*-dig pathways form dienes (**a**, **b** and **c).** 6-*endo*-dig pathways form bicyclo[4.1.0]heptane ring structure.

Introduction of a propargylic ester to the 1,*n*-enyne allows for a more complex rearrangement. Reactions involving these molecules have many seminal findings with a variety of transition metal catalysts where either a 1,2- or 1,3-acyloxy migration are possible. Crookson found that propargyl acetates will form an interesting allenyl ester consisting of a 1,3-acetoxy migration upon exposer to Ag (I) (see Figure 12).

In 1975, Ohloff et al.[15] found that carvenone and small amounts (5%) of bicyclo[4.1.0]heptane products were found from the cycloismerization of 5-acetoxyhept-1-ene-6-ynes by the use of $ZnCl_2$ (see Figure 13). In 1984, Rautenstrauch[19] also found a

similar cycloisomerization forming cyclopentenone (rather than a bicyclic structure) by reaction of 3-acetoxypent-1-ene-4-ynes with $PdCl_2$ in a Nazarov-like reaction.

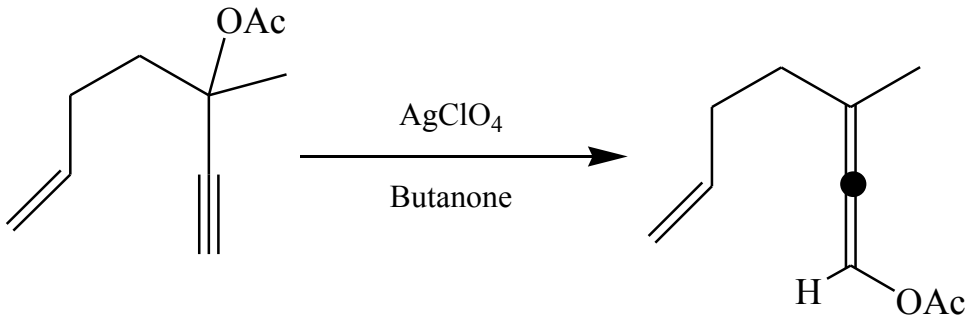

Figure 12. Silver (I) catalyzed 1,3-aceyloxy migration of propargyl acetate forming an allenyl ester

Metal-catalyzed rearrangements like this, that consist of cyclization, accompanied by ester migration have come to be called the "Ohloff-Rautenstrauch" rearrangements, after the seminal work by Ohloff[15] and Rautenstrauch[16]described above. It wasn't until later that the full appreciation of this rearrangment was understood. In 2002, Fensterband, Malacria and Marcocontelles[17] reported a similar rearrangement utilizing $PtCl_2$ to form a bicyclo[6.1.0]non-3-ene ring structure (Figure 14).

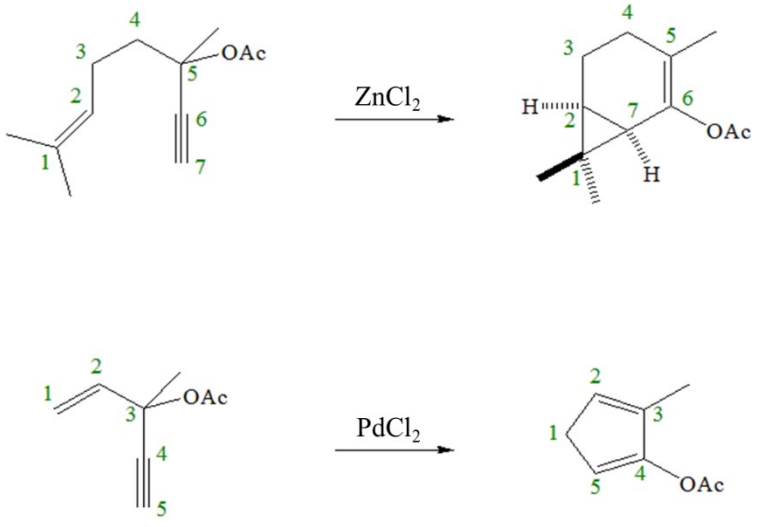

Figure 13. Seminal "Ohloff-Rautenstrauch" rearrangements. Feature cyclization and ester migration. Top: work done by Ohloff forming small amounts of a bicyclic ring structure from a 1,6-enyne. Bottom: work done by Rautenstrach forming a single ring structure from a 1,4-enyne

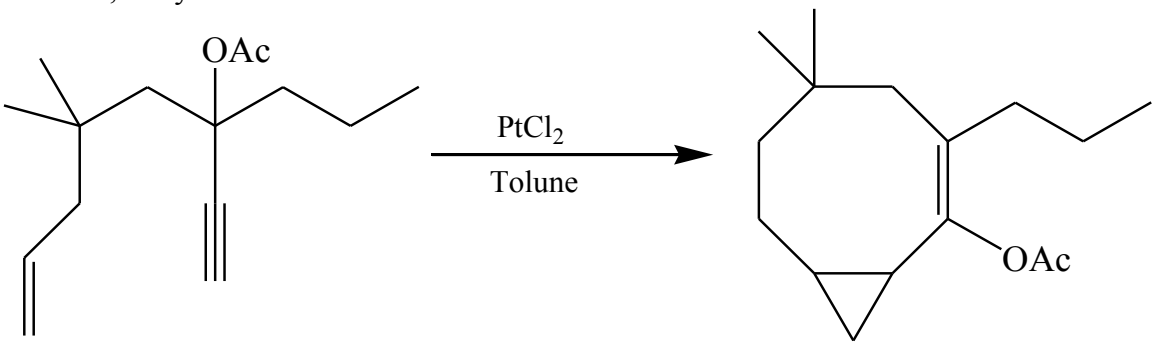

Figure 14. $PtCl_2$ catalyzed rearrangement allow easy access of a cyclopropyl fused cyclooctane structure.

The Ohloff-Rautenstrauch rearrangement is synthetically equivalent to previous methods of intramolecular cyclopropanation of α-diazoketones by copper bronze. The α-diazo-3-ketone methodology involves the use of the toxic and potentially explosive diazomethane (Figure 15)[18] so the metal-catalyzed Ohloff-Rautenstrauch rearrangement represents a significant improvement.

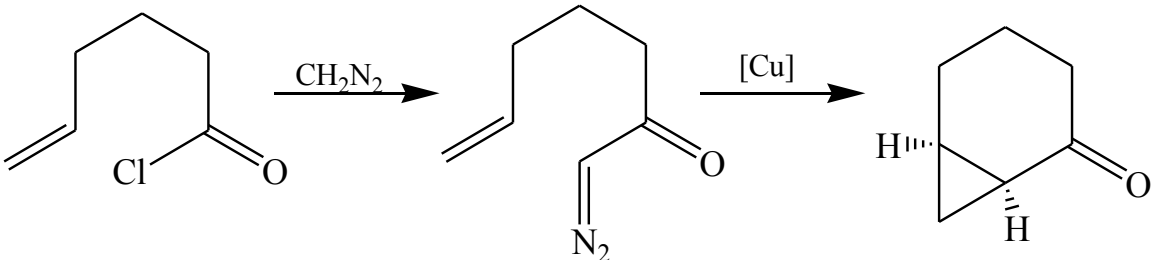

Figure 15. Synthesis of a bicyclic ring structure by the use of α-diazoketones and copper bronze.

It wasn't until 2006 that Füsrtner and Hannen showed the Ohloff-Rautenstrauch rearrangement could be achieved with a gold catalyst. Attempts to apply this rearrangement onto natural product synthesis were conducted by the Fürstner group by using easily obtained substrates. Exposure of the $PtCl_2$ catalyst to a specific propargyl acetate, obtained from the commercial product geranylacetone, afforded a mixture of products (bicyclo[4.1.0]heptane and allene acetate structures; Figure 16). These two products are very difficult to separate, so they considered the catalytic cycle and screened other catalysts. They a found that use of $AgBF_4$ gave predominantly the allene acetate. The best catalyst (providing the most selective formation of the desired bicyclic product) was $AuCl_3$ in 1,2-dicholoroenthane at room temperature. Upon work up and a few more reactions, 2-sesqucarene a component of the essential oil from the fruit *Schisandra chinensis*[19]

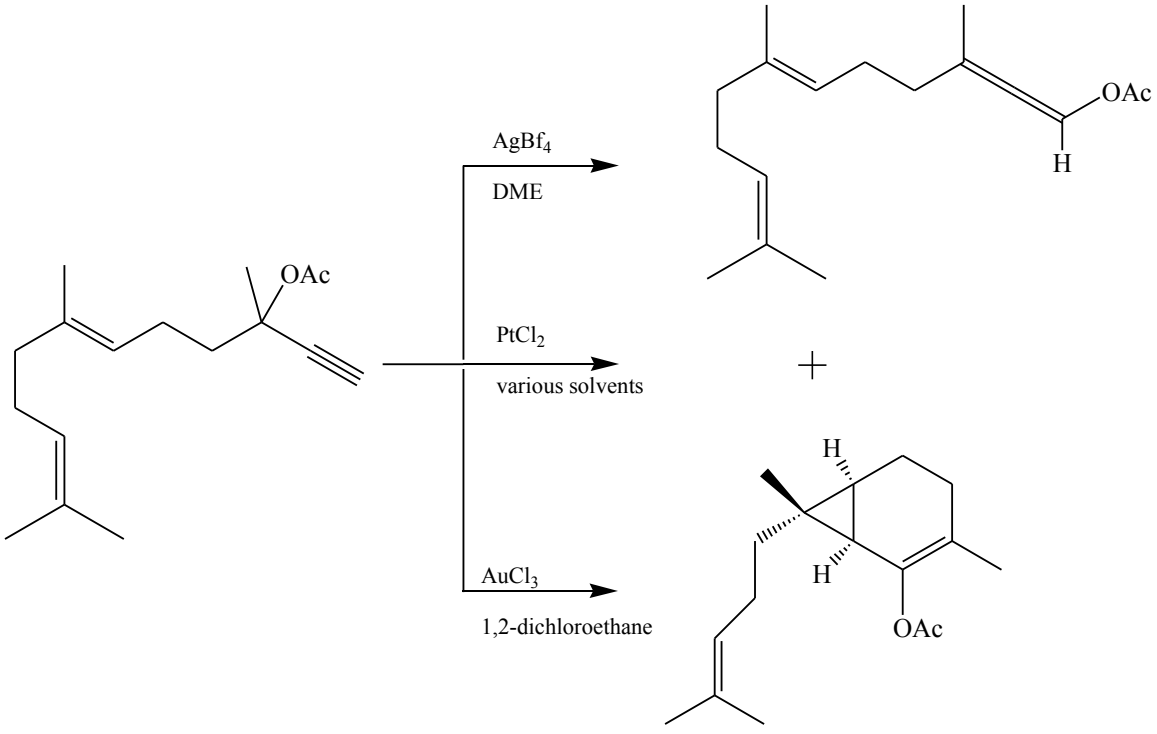

Figure 16. Rearrangement of a propargyl acetate affording a mixture of reactants when exposed to $PtCl_2$. Screening of catalysts shows a selective formation of reactants. Allene

acetate was predominate with exposure of $AgBF_4$. The desired bicyclic product was found with $AuCl_3$.

Application of this new method was utilized on a truncated reactant from Figure 16 to produce 2-carene, another naturally occurring compound. The work by Fürstner and Hannen showed that this methodology could be applied to natural product synthesis.[19] An interesting application of the above-mentioned methodology is found in the formation of a tricyclic ring structure. This method could be used to create (-)-cubebol (Figure 17), a compound from *piper cubeba L.*, patented for its applications in the flavoring industry as a "cooling" agent.[20]

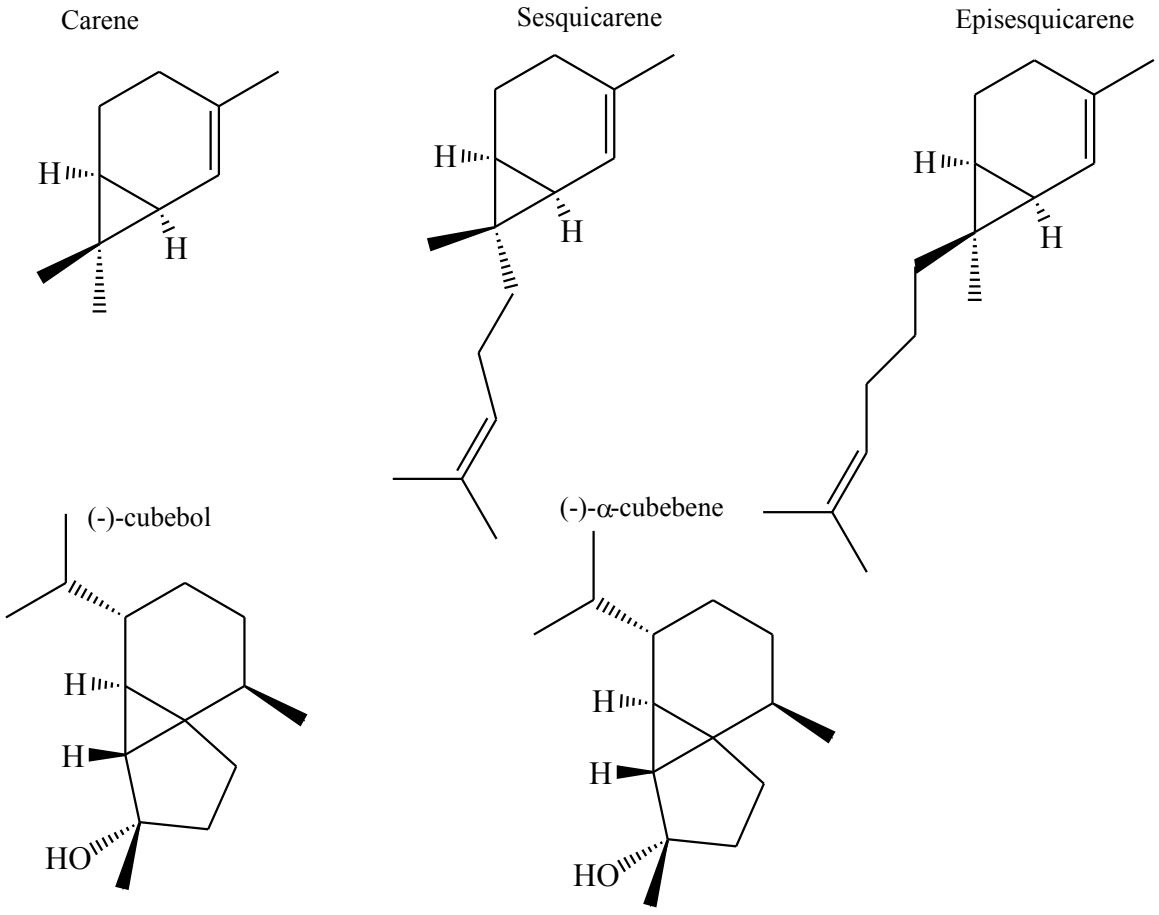

Figure 17. Natural products containing bicylo[4.1.0]heptane synthesized by methodology found by Fürstner and Hannen.

The mechanism for this gold-catalyzed Ohloff-Rautenstrauch rearrangement is proposed to proceed through two main events, cyclization (to form the bicyclic ring structure) and the migration of the acetate group (C5-O7 breaking and C6-O9 forming; numbering of atoms shown in Figure 18). Either event could in theory happen in any order thus giving us two different mechanisms that have been proposed.[19] One pathway starts with cyclization forming structure **C**, which is followed by the shifting of the acetate group (seen over structures **E** to **F**); we will call this the *"cyclization first"* pathway. The second pathway starts with the acetate group shifting (seen over structures **A** to **B**) and then the cyclization forms the product (**F**); we will call this the *"migration first"* pathway. These are only the two "main events" that must happen to fulfill the rearrangement, however, the mechanism may require conformational changes to fully complete the rearrangement.

Conclusion

The focus of this work is to investigate this rearrangement using computational methods to better understand the mechanism. This work utilized the truncated structure **A** forming the carene-like product **F** (Figure 18). The computational model will make use of a $AuCl_3$ catalyst and 1,2-dicholoroethane solvation. The next chapter will build an understanding of the computational methods used in determining whether there is a preference for "cyclization first" or "migration first".

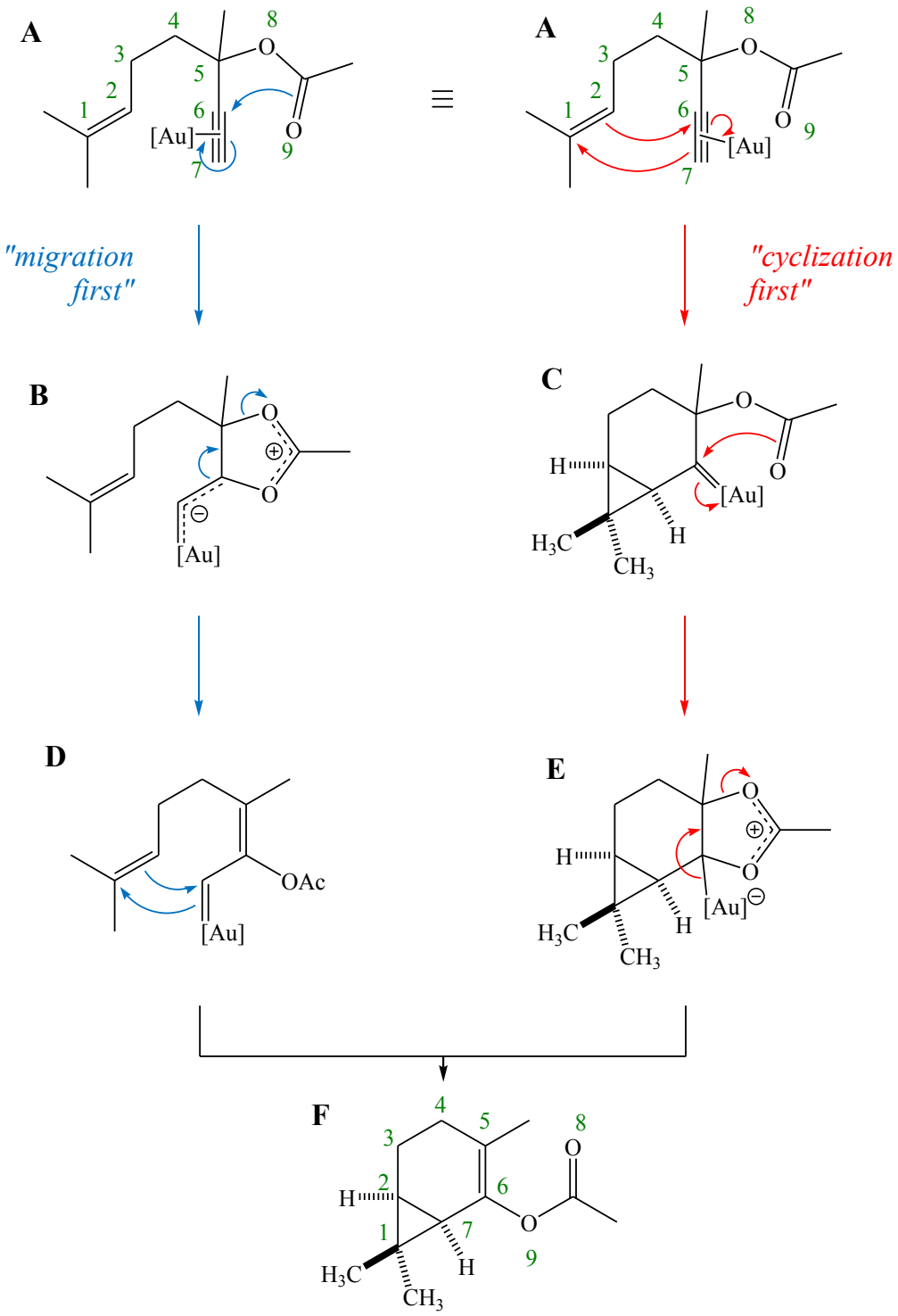

Figure 18. Proposed pathways for the gold-catalyzed "Ohloff-Rautenstrauch" rearrangement. "Migration first" starts with acetate shifting followed by the formation of the bicyclic ring structure. "Cyclization First" shows the reverse, formation of the bicyclic ring structure followed by the acetate shifting.

THEORETICAL BACKGROUND

Introduction

Reaction mechanisms are a key concept to understanding how a starting material is transformed into a product. Mechanisms rationalize movement of electrons including forming and breaking bonds.[21] If the energies related to the reactant and product are known then valuable information can be deduced such as whether the reaction is favorable ($\Delta G < 0$) or unfavorable ($\Delta G > 0$). There must be some sort of barrier to prevent the conversion of the reactant to product, otherwise there would be no reactants. This energy barrier will be called activation energy. The area at the peak of this barrier is the transition state (TS) and the size of this barrier determines the rate at which the reaction proceeds.[22]

Potential Energy Surface

Knowing the energy for every possible arrangement of a structure provides a "surface" where energy is plotted against the geometric parameters of the molecules, this is called the potential energy surface (PES). For a simple molecule, such as the diatomic AB this is very easy to visualize as there is only one geometric parameter to adjust (the bond distance between atoms A and B). As the number of atoms increases for molecules the number of geometric parameters (degrees of freedom) increases to 3N-6, where N is the number of nuclei (or 3N-5 for linear molecules), when neglecting translational and rotational movements. For a molecule with three nuclei there would be three geometric parameters that can be changed. Visualization quickly becomes a problem as each degree

of freedom needs to be plotted against energy. Therefore, for that system of three atoms four dimensions are necessary. Normally we are only concerned with one degree of freedom at a time so this is easily simplified.

Important points on the surface are stationary points, meaning that the first derivative of the potential energy with respect to all geometric parameters is zero. Minima are structures located at the lowest point in the local region of the surface where the second derivative is greater than 0. The lowest energy path connecting two minima is called the minimum energy pathway (MEP). The highest point on the MEP is a structure called a saddle point, where the second derivative is negative with respect to one degree of freedom but positive with respect to all others. This would look like a valley between two mountains, where in all directions but two (forwards or backwards) the energy increases. For the rest of this work we will call this structure the transition state structure (TSS).[23]

Quantum Chemistry

The goal of this technique is to ultimately solve the time-independent Schrödinger equation (Equation 2), the fundamental postulate of quantum mechanics, for a system of interest.

$$\hat{H}\Psi = E\Psi$$

Equation 2. Time-independent Schrodinger equation. Where $\hat{H}$ is the Hamiltonian operator, Ψ is the wavefunction of the system, and E is the energy of the system.

The wavefunction, which contains all properties of a system, is acted upon by an operator, in this case the Hamiltonian operator, giving us total energy. The typical form of the Hamiltonian operator consists of five terms: kinetic energy of electrons (T_e) and the nuclei (T_n), the attractive potential energy of electrons and nuclei (V_{en}), and the repulsive potentials of electrons (V_{ee}) and nuclei (V_{nn}).

$$\hat{H} = T_e + T_n + V_{en} + V_{ee} + V_{nn}$$

$$\hat{H} = -\sum_i \frac{\hbar^2}{2m_e}\nabla_i^2 - \sum_k \frac{\hbar^2}{2m_k}\nabla_k^2 - \sum_i \sum_k \frac{e^2 Z_k}{r_{ik}} + \sum_{i<j} \frac{e^2}{r_{ij}} + \sum_{k<l} \frac{e^2 Z_k Z_l}{r_{kl}}$$

Equation 3. Hamiltonian operator, where *i* and *j* represent all electrons and *k* and *l* are all nuclei, Z_k is the atomic number of nucleus *k*, m_e is the mass of the electron, m_k is the mass of nucleus *k*, *e* is charge of the electron, *r* is the distance between particles.

Looking at this operator, we can start to see how complex this problem of solving the Schrodinger equation can be. It includes the attractive and repulsive terms for all the particles in the wavefunction and these terms are dependent on each other's positions and movements, called correlation. This operator can be simplified if we look at the comparative mass of the electrons and nuclei. For example, for the hydrogen atom the mass of the proton is 1800 times heavier than the electron and because of this large difference in mass the electrons move much faster than the protons in the nucleus. From this we can assume that the nuclei are fixed in their positions and the electrons can "relax" instantaneously in response to the nuclear positions. This is called the Born-Openheimer approximation. This allows the kinetic energy of the nuclei to become zero and the potential energy for the nuclear repulsions at a specified geometry to become a constant.

$$\hat{\mathrm{H}} = -\sum_{\mathrm{i}} \frac{\hbar^2}{2\mathrm{m_e}} \nabla_i^2 - \sum_i \sum_k \frac{e^2 Z_k}{r_{ik}} + \sum_{i<j} \frac{e^2}{r_{ij}} + V_{nn}$$

$$\hat{\mathrm{H}}_{\mathrm{elec}} = -\sum_{\mathrm{i}} \frac{\hbar^2}{2\mathrm{m_e}} \nabla_i^2 - \sum_i \sum_k \frac{e^2 Z_k}{r_{ik}} + \sum_{i<j} \frac{e^2}{r_{ij}}$$

Equation 4. Electronic Hamiltonian operator after invoking the Born-Openheimer approximation. This operator is now based on only electrons (*i*) and the fixed positions of nuclei (*k*).

This simplifies the Schrodinger equation to a matter of describing the electrons. Another benefit from this approximation is the ability to create a PES, where the E_{elec} is found for every fixed nuclear coordinate. This concept is central to computational chemistry as it allows use to bring meaning to molecular geometries.[24]

Since we have now reduced the Hamiltonian to be based on electrons we need a function to represent the electronic wavefunction for a molecule. The problem arises with the last term in the Hamiltonian operator, calculating the effect that one electron has on another is not a trivial task. One system that can be solved is one that contains only one electron and one nucleus, a hydrogen atom. This results in the familiar hydrogenic atomic orbitals (1s, 2s, 2p, etc.). Since the wavefunction is something that is not known for larger systems it is approximated by using the hydrogen orbitals centered on nuclei in a linear combination (Equation 5).

$$\Phi = \sum_{i=1}^{n} a_i \varphi_i$$

Equation 5. Linear combination of atomic orbitals (LCAO). The wave function (Φ) is approximated by taking a sum of atomic orbitals (φ_i) at some coefficient (a_i).

In practice, this gives a way to start generating a trial wavefunction that can be used and systematically improved by minimizing the function with respect to the energy. The approximated trial wave function will always be greater or equal to the actual ground state wavefunction. This is the variational principle.[24]

Basis Sets. The basis sets used to create the molecular orbitals are functions called either Slater-type orbitals (STOs) or Gaussian-type orbitals (GTOs).

$$\eta^{STO} = Nr^{n-1}e^{-\zeta r}Y_{lm}(\Theta, \varphi)$$

$$\eta^{GTO} = Nx^{l}y^{m}z^{n}e^{-\alpha r^2}$$

Equation 6. General forms of Slater-type orbitals (STO) and Gaussian-type orbitals (GTOs). *N* is normalization factor. Θ, *r*, and φ are spherical coordinates and *Y* is angular momentum. *n*, *l*, and *m* are quantum numbers. *x*, *y*, and *z* are cartesian coordinates.

Though STOs are more like hydrogen atomic orbitals with a cusp at r = 0 and decay at an appropriate rate, they are very hard to compute. GTOs lack some feature of hydrogen orbitals as at r = 0 the slope is 0 and they decay too quickly. Since STOs present problems in calculations, the use of a contracted Gaussian-type orbitals is preferred. The minimum basis set is STO-3G where three Gaussian functions are combined to form a basis function that resembles an STO. This basis set is known as single-ζ where it contains only one basis function. Double-ζ, instead of having a single contracted basis set of three single Gaussian functions, has two basis sets where one is made of two Gaussian functions and the other is made of one Gaussian function. An example of this would be a basis set from Dunning such as cc-pVDZ. Breaking up functions allows for more flexible description of the electrons. Chemists understand that (generally) the valance electrons are more important in describing chemical reactivity

than the core electrons, for this reason more flexibility in the valance shell would be useful. Split-valence basis sets allow for this description. The most common examples of these basis sets are those created by Pople. Pople basis sets are written out in the format #-##G where the digit in the front is the number of GTOs that are contracted for the core orbitals, the number of digits after the dash are the number of contracted Gaussian type orbitals used with the number of the digit being how many functions each is made up of. For example, the 6-31G basis set has 1 basis function with 6 contracted GTOs describing core electrons while the valance shell has 2 basis functions, with one being made of 3 contracted GTOs and the other having just 1 GTO.[24]

For very large atoms containing many electrons the number of Gaussian functions required becomes a problem for computational cost. To fix this problem while retaining the accuracy of the system, one can replace the non-reactive core electrons with a function that represents the nuclear-electronic core, called an Effective Core Potential (ECP). There are two main methods of modeling the core: either include everything into the core except the outermost valence electrons or to model everything but the two outerost shells. As mentioned in Chapter 1, large atoms also show relativistic effects. ECPs accurately incorporate relativistic effects in the core. A popular ECP was developed by Hay and Wadt, called the Los Alamos National Laboratory with a double-ζ basis set (LANL2DZ). For gold, this replaces 60 core electrons.

Slater Determinant. The major problem now is the fact that electrons are fermions so this wavefunction needs to be antisymmetric with respect to the exchange of two electrons. This problem is fixed by invoking a Slater determinant.

$$\psi = \frac{1}{\sqrt{N!}}\begin{bmatrix} \chi_1(1) & \cdots & \chi_N(1) \\ \vdots & \ddots & \vdots \\ \chi_1(N) & \cdots & \chi_N(N) \end{bmatrix}$$

Equation 7. Slater determinant for creating an antisymmetric trial wavefunction. N is the number of electrons and χ is the spin-orbital.

Electrons are represented by the columns in the determinant and swapping any two electrons (columns) leads to an inversion of the sign of the wavefunction. Using these methods allows for the creation of a suitable molecular orbital that is antisymmetric due to the Slater determinant and is minimized by using the variational principle.

Hartree-Fock Method. So now we have approximations for both an electronic wavefunction and a Hamiltonian based on only the electrons and the fixed coordinates of the nuclei. This method is called the Hartree-Fock method. This method is the cornerstone for wavefunction based methods. To approximate the final problem with the Hamiltonian (the potential from the repulsions of the electrons) the Hartree-Fock method creates a mean-field approximation where each electron moves independently of others in an average field created from the other electrons. This creates an operator like the Hamiltonian, in using the one-electron Hamiltonian along with the addition of the Hartree-Fock potential, called the Fock operator.[24]

$$f_i = -\frac{1}{2}\nabla_i^2 - \sum_k \frac{Z_k}{r_{ik}} + V_i^{HF}$$

Equation 8. Fock operator based on one electron (i) and the positions of the nuclei (k) with the addition of the Hartree-Fock potential (V^{HF}).

One of the main problems with this method is that the total energy is always higher than the actual energy of the system. This is due to the approximation that the

electron is interacting with the rest of the electrons in a mean field of the total electrons. This error is small but can have a large effect on certain properties calculated for the system.

Density Functional Theory (DFT). Hohenberg and Kohn published two theorems that made DFT useful. The first theorem proves that an electron density can give a unique external potential, which provides a Hamiltonian and a wavefunction and in turn give a unique energy for that density. The second theorem shows that the variational principal can be applied to electron densities so that a trial density can be approximated and will be higher than or equal to the ground state energy.[24]

Kohn and Sham developed a method for DFT where the system is built upon a set of noninteracting orbitals and each electron is in an average repulsion field from the remaining electrons (similar to the approximations in HF). The difference is that in DFT an exact answer is theoretically possible. However, a description for the exchange-correlation energy needs to be approximated. The total energy of this system can be broken up into parts shown in Equation 9.

$$E[\rho] = T_s[\rho] + \int [V_{ext}(r) + J(r)]\rho(r)dr + E_{xc}[p]$$

Equation 9. Energy of the system based on Kohn-Sham noninteracting orbitals. $T_s[\rho]$ is the electron kinetic energy for the system where the density (ρ) matches the real system. $J(r)$ is the coulomb interaction between electrons and V_{ext} is the external potential from the nuclei. The final term E_{xc} contains all other contrbutions to the total energy that are not known.

The exchange- correlation energy (E_{xc}) is the one term that is not known and prevents the exact solution using this method. Thus, to calculate the energy based on this

method, an approximation for this term is needed. The term contains non-classical electron-electron interaction along with the self-interaction corrections that arise from assuming a non-interacting system. The problem is that there is no systematic way to approximate this term nor is it known what form it should take.[24]

Functionals. The starting point for this is using a uniform gas as the electron density known as the local density approximation (LDA) to approximate E_{xc}. This is a rough approximation since in a molecule the electrons are not uniformly spread out but show rapid variations of densities.[24]

The next step up from this is to use an electron density that utilizes a gradient. This allows for a difference in electron density in different parts of the molecule. This method is called the generalized gradient approximation (GGA).[24] Normally this method breaks the E_{xc} into E_x (exchange) and E_c (correlation) terms and approximates them individually. Building on this, the exchange portion can be better described with the inclusion of the exchange portion from HF, which is described exactly. A mixture of DFT and HF exchange is found to provide the best results, these are known hybrid functionals. The best example of this is the combination of Becke's, three-parameter exchange and Lee, Yang and Parr's correlation functional (B3LYP)[25]. This method is a very widely used functional providing reasonably accurate results for many systems. B3LYP approximates the exchange-correlation using a mixture of HF and LDA exchange, Becke 1988[26] exchange and LYP correlation[27] (Equation 10).

Though this functional has seen wide use in the recent past, it is starting to fall out of favor as its limitations become more apparent. The main problem is when describing

long and short range dispersion forces[28,29], which becomes a larger error as the size of the system increases, van der Waals interactions[30], and extend π-systems[31].

$$E_{XC}^{B3LYP} = E_{XC}^{LDA} + a_o(E_X^{HF} - E_X^{LDA}) + a_x E_X^{B88} + a_c E_C^{LYP}$$

Equation 10. Exchange-correlation approximation for B3LYP. Three empirical parameters are fit to atomization energies, ionization potentials, proton affinities and atomic energies. $a_o = 0.20$, $a_x = 0.72$, and $a_c = 0.81$.

More modern funtionals start to include additional terms to help fix this drawback. Two functionals starting to see more use in recent years are B2PLYP[32] and M06[33]. Grimme took an approach based on the combination of Becke (B1988), LYP correlation, HF exchange and perturbative second-order correlation(MP2) to form B2PLYP; (Equation 11). This functional is considered a double-hybrid functional with the mixing of DFT, HF and MP2 method.

$$E_{XC}^{B2PLYP} = (1 - a_x)E_X^{GGA} + a_X E_X^{HF} + bE_C^{GGA} + cE_c^{MP2}$$

Equation 11. Exchange-correlation approximation for B2PLYP. This functional does this calculation in two parts, the first part includes the non-perturbative portion. The result from this is then used in the perturbative portion

This functional has a drawback compared to B3LYP as it is costlier method (required more time). Truhlar developed a functional based on meta-GGA and HF. This method has been parametrized for ground-state energy databases for both main-group and transition metals, bond lengths, and vibrational frequencies

$$E_{XC}^{M06} = \frac{x}{100} E_x^{HF} + \left(1 - \frac{x}{100}\right) E_X^{mGGA} + E_C^{mGGA}$$

Equation 12. M06 hybrid approximation for exchange-correlation energy. The exchange is approximated by a portion of HF and DFT exchange and correlation from DFT.

The M06 functional is stated to be good for studying organometallic systems.[33] Now the problem, it would seem, is which method is better, as there is not one functional that works in all situations. These two functionals show similar ways to approximate $E_{XC,}$ using both HF and DFT in proportions parameterized to sample systems. The next chapter discusses the choice of functional for this work.

Dispersion Correction. As was mentioned before the B3LYP functional has trouble with describing dispersion in a system. The other two functionals (B2PLYP and M06) have incorporated more parameterization and have less issue with dispersion. Methods have been developed to include a better description of these weak interactions, improving description of larger molecules and organometallic systems. Better description of these attractive effects has a great effect on both the physical and chemical properties of the systems.[34] A popular choice for dispersion corrections is the method of Grimme[35] (D3). The use of dispersion corrections is denoted as DFT-D3 where DFT is the functional being used, such as B3LYP. This current iteration is accurate for all chemically relevant elements on the periodic table (nuclear charge 1-94) and has improved description for "light" molecules and for "heavier" metallic systems. The method calculates the total corrected energy by subtracting the dispersion correction from the regular DFT energy calculated form the functional used. The dispersion corrections are described by Equation 13, which includes terms for two- and three-body interactions.[24]

$$E_{disp} = \sum_{AB} \sum_{n=6,8,10,\ldots} s_n \frac{C_n^{AB}}{r_{AB}^n} f_{d,n}(r_{AB}) + E^{(3)}$$

Equation 13. General form of dispersion correction showing expanded two- and three-body terms ($E^{(3)}$) Sums over all atoms pairs (A, B). C_n^{AB} is the dispersion coefficient for each pair. r_{AB} is the internuclear distance of atoms A and B. $f_{d,n}(r_{AB})$ is the dampening function.

Solvation. Since most chemical reactions take place in solutions, the effects from solvation should also be considered to generate data that are more consistent with experiment. Without the inclusion of a solvent the calculation is conducted in the gas-phase. There are two approaches to incorporating solvent, the first is to add explicit solvent molecules and run the calculation. But how many molecules of solvent do you need to include? Many solvent molecules could be needed to accurately represent this system and this will make the calculation run for a much longer time (if it even finishes). An alternative approach is to implicitly model the solvent. At a basic level this method places the molecule in a cavity within a continuous dielectric medium with a dielectric constant equal to that of the solvent being studied. If specific solvent-solute interactions are not important to the description of a system then this so-called "implicit" solvent model is acceptable. Definition of the cavity the molecule is placed in is important to modeling. It is accepted that the solvent cavity should have some physical meaning where it should match the molecular shape. Deviation of an accurate cavity would lead to unrealistic charge distribution and would affect both the geometry and the energy of the system. To model this effectively, the cavity is shaped by using atom-centered spheres with a rational selection of radius, such as van der Walls radius.[24]

Conclusion. This chapter should give a basic understanding of the methods used during this work. For those interested in developing further understanding see reference

24. The next few chapters will describe the use of these methods to elucidate the mechanism of gold (III)- catalyzed Ohloff-Rautenstrauch rearrangement and whether there is a preference for “cyclization first” or “migration first”.

GAS PHASE CALCULATIONS

Herein appears a description of the gold(III)-catalyzed Ohloff-Rautenstrauch rearrangement of the propargylic ester forming the acylcarene product in the gas-phase. The initial starting point of this project is aimed at determining the minimum energy pathways for each of the "migration first" and "cyclization first" mechanisms in the "gas-phase". This type of calculation essentially places the molecule into a vacuum, which does not account for any intermolecular stabilization of charges.

Methods

To model a problem such as this the first thing that needs to be considered is what functional and basis set will be used. Since there is no perfect model chemistry for every system, studies are done with various functionals and basis sets.

A few benchmark studies on gold-catalyzed processes have been done. Extensive work done by Chen and Yao[36] looking into the binding of various gold(I) and gold(III) catalysts onto ethene, ethyne, and allene aimed at accurate reproduction of binding energies and geometries. The geometries and binding energies were tested with various methods against very high level coupled cluster methods [CCSD(T)]. From this study, they found that methods that showed accuracy in describing geometries correlate with those that provide accurate energies. The hybrid-GGA PBE0 and double hybrid B2PLYP were found to most accurately model these systems' geometries. Double hybrid methods B2PLYP and B2GPLYP provided similar energies to the CCSD(T) methods. The

inclusion of dispersion corrections empirically increased accuracy of these double hybrid methods.

Belpassi and Belanzoni[37] (in 2014) performed an analysis on the gold(I)-catalyzed hydroamination of alkynes. This work provided benchmark calculations for determining the most accurate model chemistry for both geometries and energies compared to DF-LCCSD(T) and to CCSD(T) "gold standard" calculations. They concluded that the B2PLYP functional is the best for calculating both geometries and energies, along with at least a triple-ζ basis set with polarization (they used def2-TZVP). They also showed that performing geometry optimization with a less expensive functional, such as B3LYP, then performing a single point calculation with B2PLYP provided almost identical results.

From the select benchmark studies described above, we chose to determine the minimum energy pathway by first optimizing structures with the B3LYP density functional then again using these geometries with the B2PLYP functional, both using 6-31G(d) on non-metal atoms (hydrogen, carbon, oxygen, and chlorine) and the double-ζ quality effective core potential and associated pseudopotential of Hay and Wadt (LANL2DZ)[38,39] on the gold atom. We performed all calculations using Gaussian09.[40] This model chemistry will be called B2PLYP/6-31G(d)-LANL2DZ. Using a smaller basis set to determine geometries of the structures helps to reduce computational cost. Figures display geometries optimized at this model chemistry. Frequency analyses were performed at the same level to determine the identity of each stationary point as well as to determine the zero-point energy corrections and Gibbs energy corrections at 25˚ C. Intrinsic reaction coordinate (IRC) calculations were performed on transition state structures (TSS) to unambiguously determine the minima associated with each.

After proper geometries were determined, energies were calculated by performing single-point calculations using a larger basis set (Weigend and Ahlrichs' def2-TZVP)[41] and including of dispersion corrections (D3) on the B2PLYP density functional. Energies listed in figures are relative to structure **G4** (Figure 20) from B2PLYP-D3/def2-TZVP electronic energies with unscaled zero-point energy correction from B2PLYP/6-31G(d)-LANL2DZ (≈ ΔH). Energies that appear in italic text are B2PLYP-D3/def2-TZVP electronic energies with the Gibbs corrections calculated from the B2PLYP/6-31G(d)-LANL2DZ model chemistry (ΔG).

Results

Overall Reaction. In the gas-phase, the B2PLYP-D3/def2-TZVP//B2PLYP/6-31G(d)-LANL2DZ model chemistry found that converting the propargylic ester (**G1**; Figure 19) to the acetylcarene (**G2**; Figure 19) is exothermic (-27.0 kcal/mol, energy of product relative to the reactant without accounting for the catalyst).

Migration first pathway. The migration first pathway, as its name implies, is characterized by the shifting of the acyl group first, followed by the formation of the ring structures. The MEP starts with the gold(III) chloride (**G3**; Figure 19) complexing to the propargylic ester (**G1**; Figure 19) to form the gold(III) η^2-complex with the alkyne (**G4**). The gold complexes the "underneath" the molecule. This binding is *anti* to the acetoxy carbonyl oxygen allowing the alkyne to be activated toward nucleophilic attack of the oxygen.

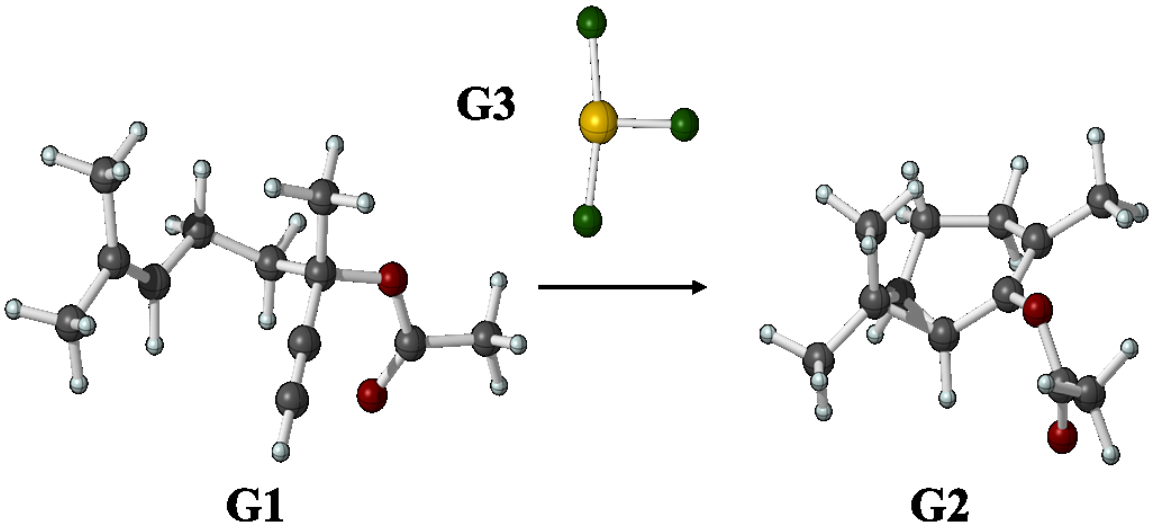

Figure 19. Gas-phase structures of overall reaction.

This binding allows for nucleophilic attack of the oxygen initiating the acyl group migration. The carbon-oxygen distance, denoted in the green line in **G4**, decreases from 2.97 Å (**G4**) → 2.29 Å (**G5**‡) → 1.45 Å (**G6**) seen in Figure 20. At the same time that the acetoxy carbonyl oxygen comes in to attack, the gold catalyst slides towards the terminal end of the alkyne. The result of this addition is witnessed in the alkyne as the C≡C distance has lengthened slightly (now consistent with that of an alkene). The nucleophilic attack proceeds through a low energy barrier (4.1 kcal/mol) and is exothermic (-9.8 kcal/mol). This forms a cyclic oxocarbenium ion (**G6**). The TSS for this step is the highest energy step for this pathway, which would normally indicate that it's the rate-limiting step of this pathway.

Following the addition of the acetoxy carbonyl oxygen, is breaking of the carbon-oxygen bond of the adjacent atom (in **G4** → **G6**). The bond is seen to break over structures **G6** → **G7**‡ → **G8** as the bond lengthens from 1.54 Å to 2.98 Å (as denoted in **G6** and **G8,** respectively). This step is mildly exothermic (-4.6 kcal/mol) and has a low

energy barrier (4.1 kcal/mol). This bond breaking reforms the acetoxy carbonyl oxygen and generates an aurodiene, completing the migration step of this pathway in a stepwise fashion.

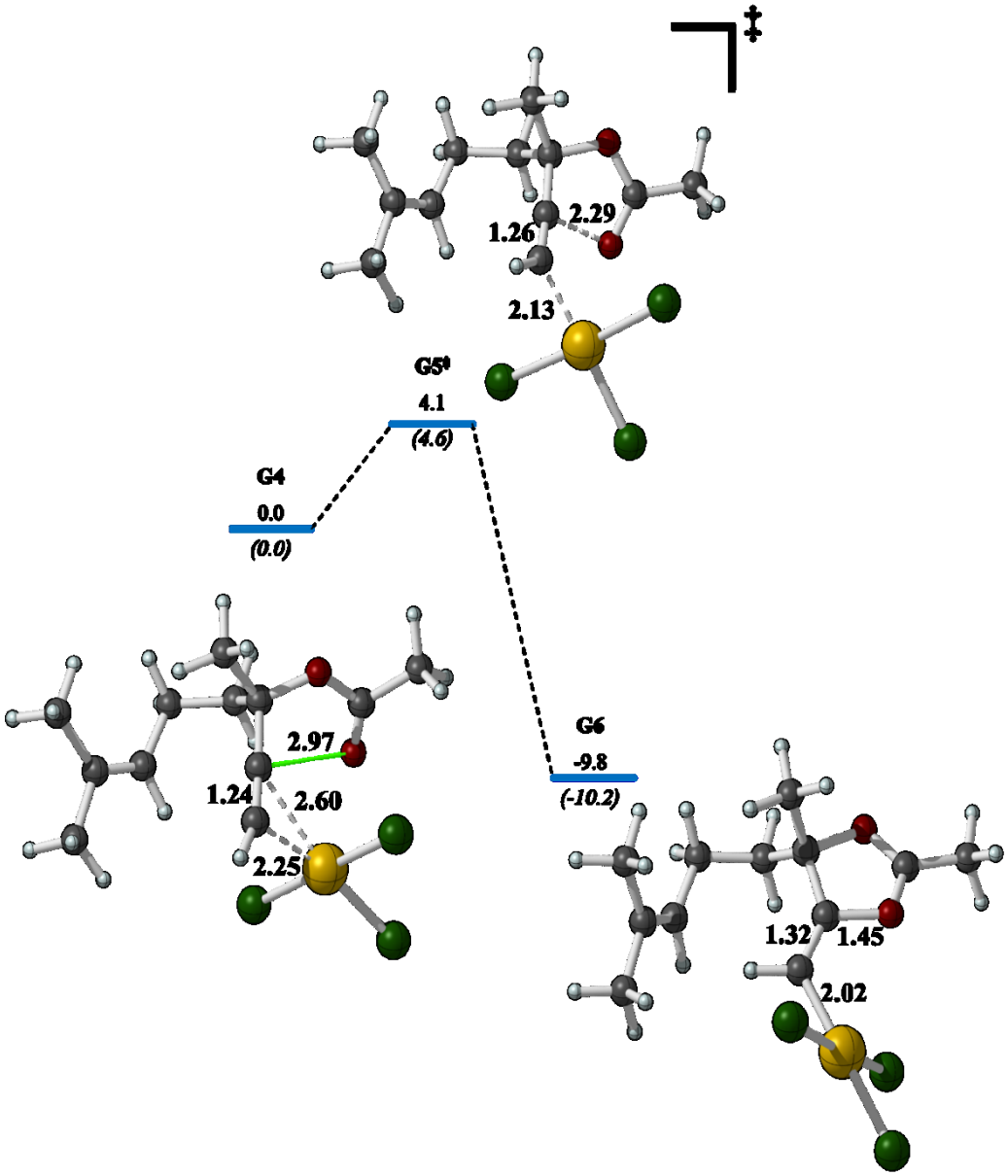

Figure 20. Beginning steps of the "migration first" pathway. Showing rate-limiting step of the initial acyl-group migration. Select bond distances are shown in angstroms (Å), energies shown are electronic energies with addition of zero-point correction (≈ΔH; Gibbs free energies are shown in italic) relative to **G4**

The ligand plane on the gold(III) in **G8** is positioned in a way that a chlorine is pointed towards the dimethyl alkene which is sterically hindering the attack of the alkene. To allow the attack, the ligand plane rotates around the dihedral Cl1-Au2-C3-C4 (see Figure 21 for numbering in blue) going from 52˚ to 42˚ (Figure 22). Along with this the acetoxy group rotates at the same time (seen as the acetoxy carbonyl oxygen moves more towards the terminal carbon end, **G8** → **G10**). This step is nearly barrierless (0.1 kcal/mol) and is only very slightly exothermic (<1 kcal/mol).

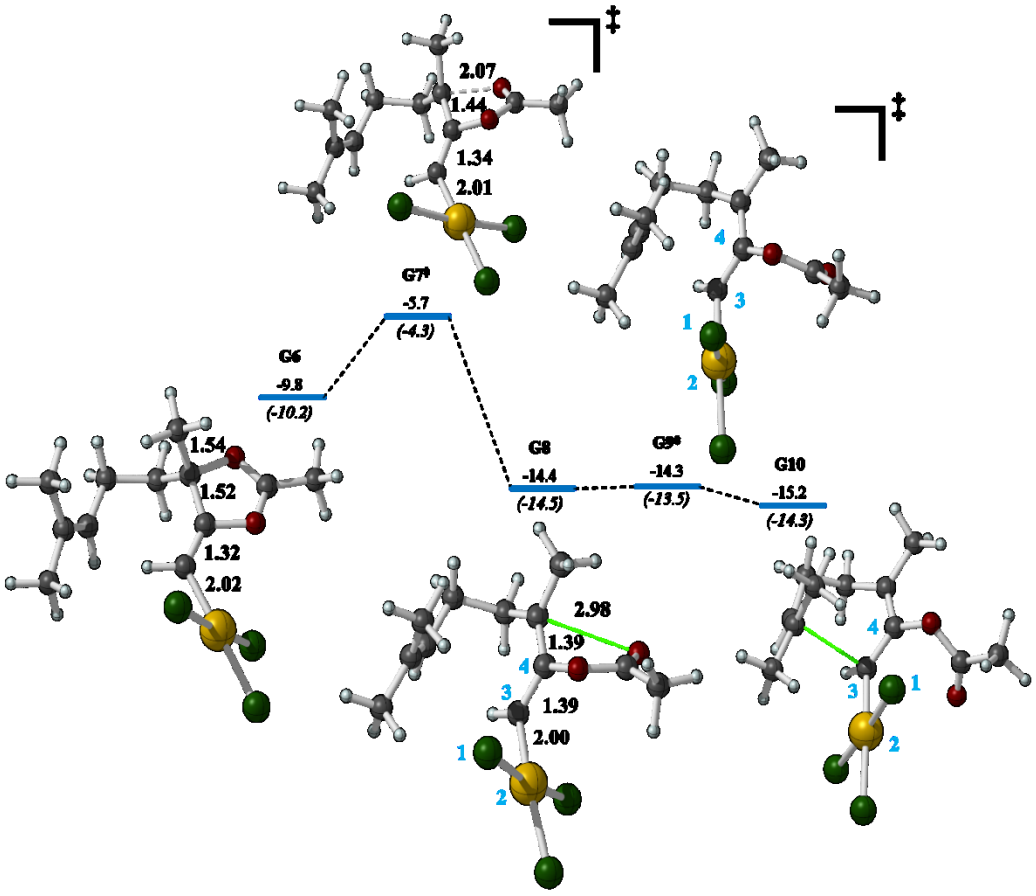

Figure 21. Final acyl-migration step in the "migration first" pathway. Alternate views of **G8** and **G10** showing conformational change in Figure 22. Select bond distances are shown in angstroms (Å), energies shown are electronic energies with addition of zero-point correction (≈ΔH; Gibbs free energies are shown in italic) relative to **G4**

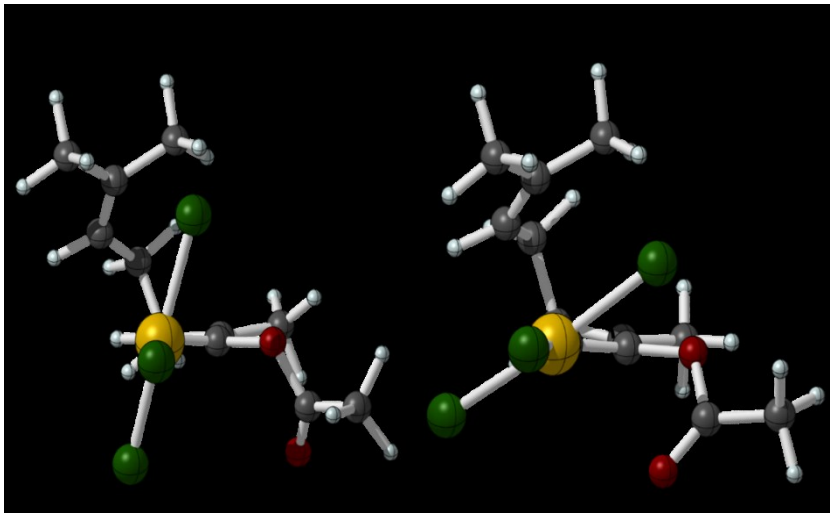

Figure 22. Alternate view of conformational change converting **G8** to **G10**. The Cl1-Au2-C3-C4 dihedral angle changes from 52˚ to 42˚.

After this conformational change (**G8** to **G10**) the cyclization can proceed. The formation of the bicyclic ring structure happens in a stepwise fashion with the electrophilic addition of aurodiene (**G10**) to the distal dimethyl alkene generating the 6-membered ring first, along with the formation of an aurocyclobutane ring structure (**G12**). Generation of this structure is exothermic (-8.6 kcal/mol) and creates a stable structure with this minimum being one of the lowest energy on this pathway (**G14** is a modest 1 kcal/mol lower). The reductive elimination of the gold catalyst from the aurocyclobutane ring has the largest single step energy barrier (13.2 kcal/mol) and is only slightly exothermic (1 kcal/mol) forming **G15**. Structure **G15** is the completed product with the catalyst complexed to the oxygen (shown in Figure 23). Structure **G14** and **G15** have the lowest energy of this pathway and might signify a sink in the catalytic cycle for this pathway. Overall, this cyclization step occurs in a stepwise manner with the formation of the 6-membered ring first, then the 3-membered ring interrupted by the elimination of the gold catalyst from the aurocyclobutane ring.

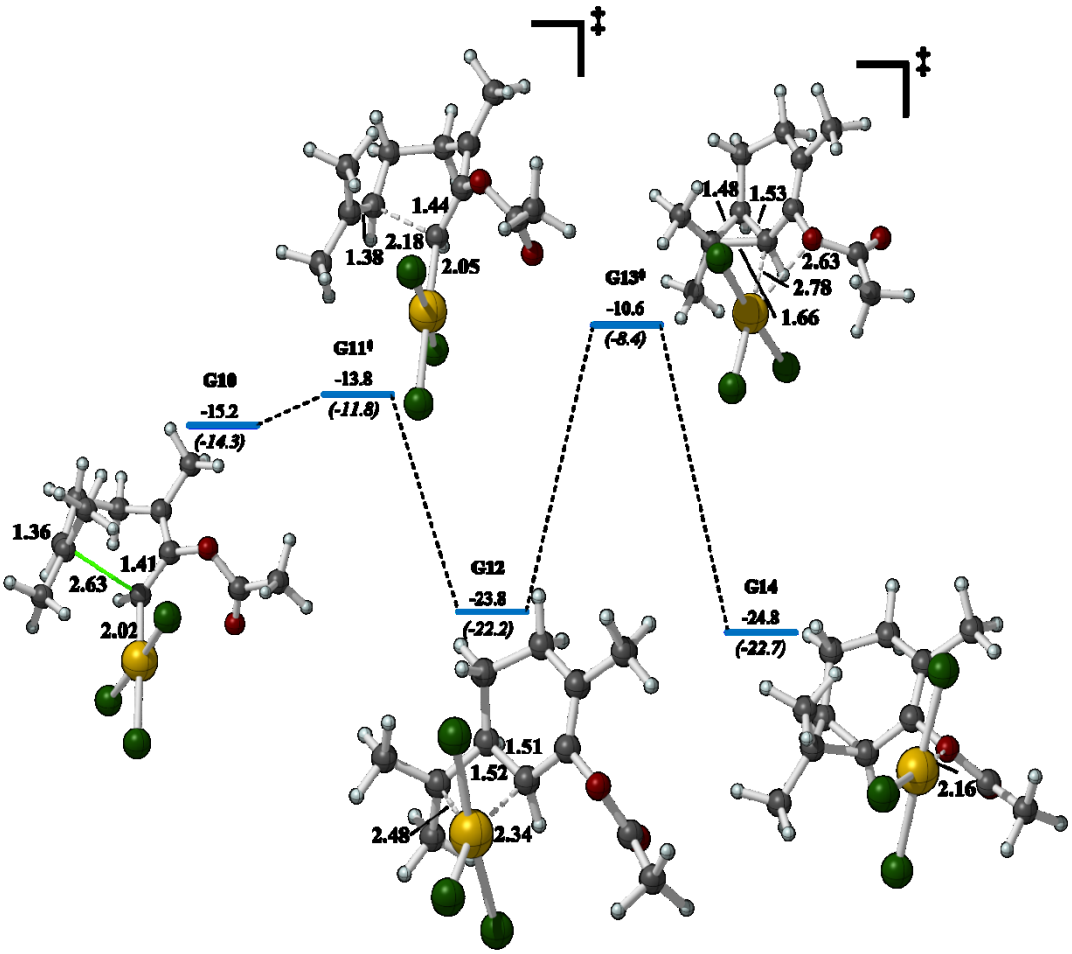

Figure 23. Cyclization steps of the "migration first" pathway seen as a stepwise formation of the bicyclic ring structure. Select bond distances are shown in angstroms (Å), energies shown are electronic energies with addition of zero-point correction (≈ΔH; Gibbs free energies are shown in italic) relative to **G4.**

Cyclization first pathway. This pathway is characterized by ring formation followed by acyl-migration. The formation of the ring is initiated by gold (III) chloride (**G3**; Figure 19) binding as an η^2-complex to the alkyne on the propargylic acetate (**G1**; Figure 19), where the catalyst is "above" the molecule, so that it is *anti* to the distal alkene (forming **G15;** compare this to the "migration first" pathway where the gold is *anti* to the acyl group, **G4**; Figure 20). Binding in this manner activates the alkyne so that the dimethyl alkene attack is preferred over the carbonyl acetoxy oxygen.

Once the alkyne has been activated by the catalyst the alkene can come in and attack through a low energy barrier (4.1 kcal/mol) that results in formation of the three- and the six-membered rings in a concerted fashion. At the same time the catalyst slides from the terminal end of the alkyne to the internal carbon (forming **G17**; Figure 24). This step is moderately exothermic (-19.2 kcal/mol). The cyclization in this pathway proceeds in one step, whereas in the "migration first" pathway the step is interrupted by the formation of an aurocyclobutane ring structure.

The next major step is the shifting of the acyl group. This step is initiated by the nucleophilic attack of the carbonyl oxygen on the carbene-gold complex (shown over **G17** → **G18**‡ → **G19** by the decreasing carbon-oxygen distance 2.96 Å → 2.34 Å → 1.53 Å), forming a cyclic oxocarbenium ion (**G19**). This step is mildly exothermic (-10.8 kcal/mol) with a low energy barrier.

To complete the migration step, a conformational change is needed to orient the gold(III) chloride antiperiplanar to the carbon-oxygen bond that needs to be broken. This conformational change can be described by a simultaneous change involving the rotation and movement of the square-planer gold ligand plane. The major change is the rotation of the ligand plane on the catalyst about the molecule allowing C5 to move past the chlorine on the catalyst. This is illustrated in Figure 25, where dihedral rotation (Cl1-Au2-C3-C4 going from -44˚ in **G19** to 32˚ in **G20**‡ to 34˚ in **G21**), allows gold to move into a relatively *anti*-position with respect to the oxygen.

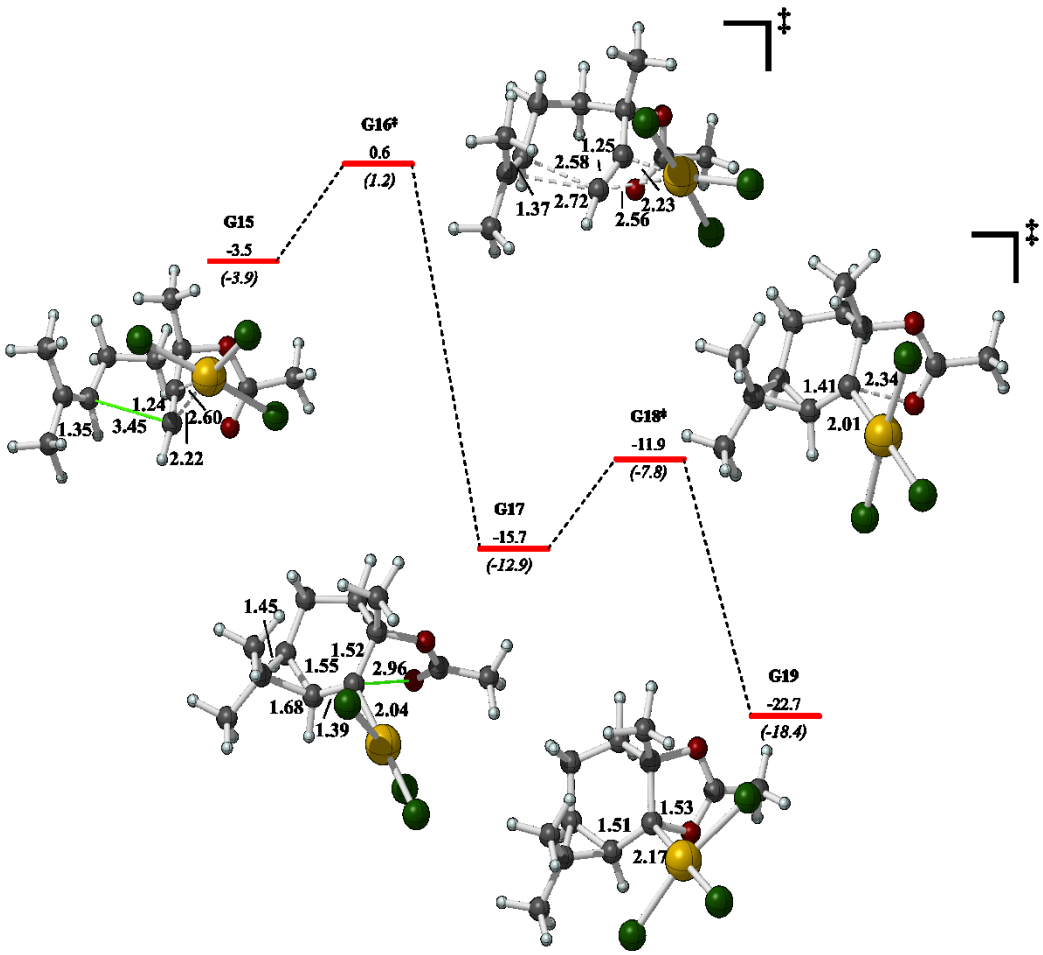

Figure 24. Cyclization and initial migration steps in the "cyclization first" pathway, showing concerted formation of the bicyclic ring structure and initial attack for acyl-migration. Select bond distances are shown in angstroms (Å), energies shown are electronic energies with addition of zero-point correction (≈ΔH; Gibbs free energies are shown in italic) relative to **G4**

This movement of the catalyst into the *anti*-position is seen over the dihedral Au2-C3-C4-O6 going from 83˚ in **G19** to 112˚ in **G20**‡ to 147˚ in **G21** but never able to fully move into the anti-position due to steric interaction between **C7** and the catalyst

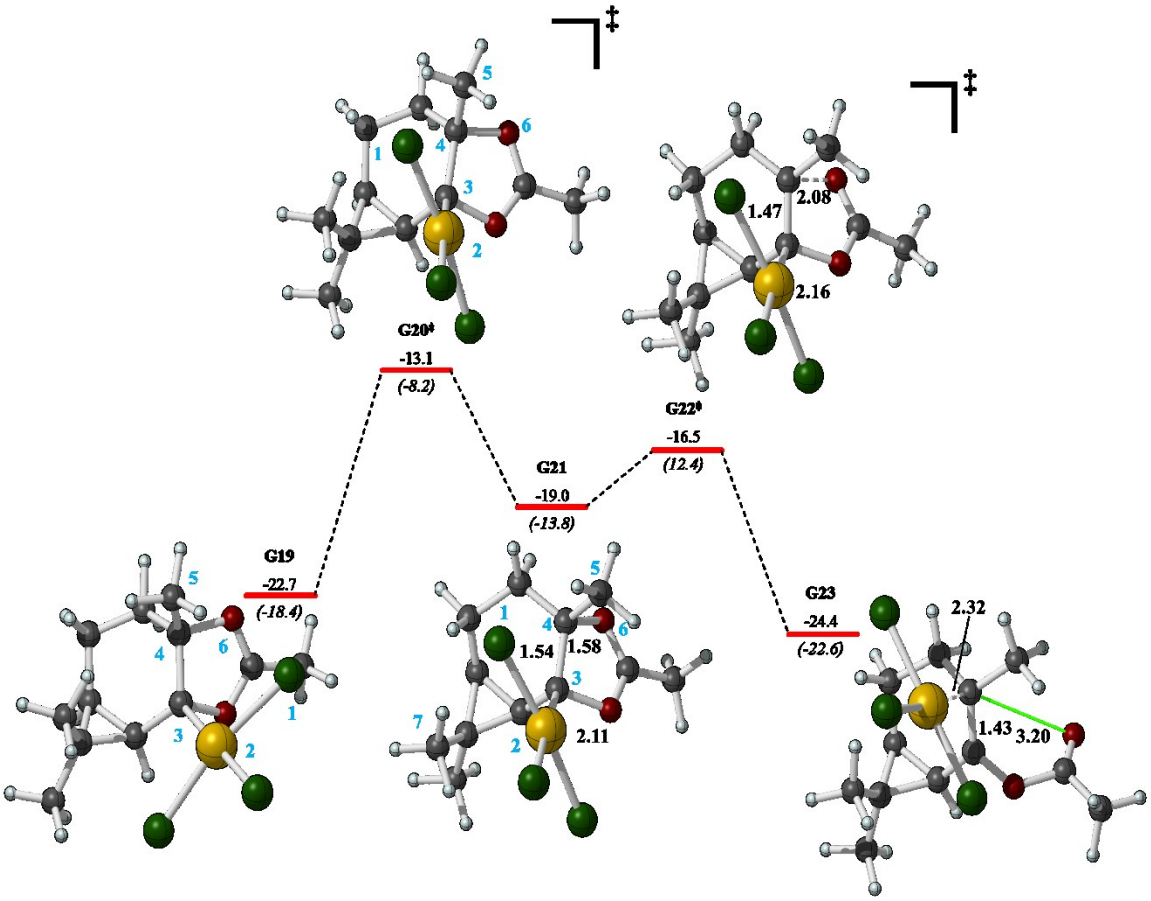

Figure 25. Completion of the migration step in the "cyclization first" pathway. Conformational change is required to move the catalyst to *anti* with respect to oxygen followed by final step in acyl-migration. Select bond distances are shown in angstroms (Å), energies shown are electronic energies with addition of zero-point correction (≈ΔH; Gibbs free energies are shown in italic) relative to **G4**

The final step of this pathway is the breaking of the carbon-oxygen bond that forms a carbonyl oxygen again (**G23**). Interestingly, the catalyst binds to the newly formed double bond, which differs from the other pathway where the gold catalyst complexes the C-O-C oxygen.

Conclusion

Gas-phase structures and energies for both pathways have been determined and presented in this chapter at the B2PLYP-D3/def2-TZVP//B2PLYP/6-31G(d)-LANL2DZ level of theory. Both pathways feature multiple steps with low to moderate energy barriers (most are exothermic). Surprisingly, the highest energy TSS is the initial nucleophilic attack in either pathway. The problem arises that both highest energy TSS are very similar in their energy ($\Delta\Delta H^{\ddagger} < 5$ kcal/mol), even though they represent very different processes. At this point, it is not clear if there is a large preference for either pathway. Experimentally this reaction was carried out in dichlorethane as the solvent. The gas-phase calculations presented herein will not properly describe solvent stabilization of charges (an important short-coming since in both pathways an ion is formed). In the next chapter, we will present calculations that more accurately represent the experimental environment by incorporating solvent implicitly.

SOLVENT PHASE CALCULATIONS

To more accurately model the experimental conditions described by Fürstner and Hannen[19], a solvent must be considered. In the reaction being studied, the solvent used was 1,2-dichloroethane. In chapter 3 the pathways were elucidated in the gas-phase; here structures will be refined by implicit inclusion of 1,2-dichloroethane.

Methods

The computational methods used for this part of the project are similar to the those describing the gas-phase pathways, amended by introducing a solvent model. Geometries were determined using B3LYP and B2PLYP density functionals. A 6-31G(d) basis set for "lighter" atoms (H, C, O, Cl), and the LANL2DZ basis set for gold. The default implicit solvent model (IEFPCM)[42] of the Gaussian09 suite was used to model 1,2-dichloroethane. The B3LYP functional was used to first optimize the structures quickly then they were reoptimized using the higher level functional B2PLYP to more accurately calculate the geometries. This model chemistry will be refered to herein as IEFPCM-B2PLYP/6-31G(d)-LANL2DZ. Single-point energy calculations were performed utilizing the B2PLYP density functional, the basis set of Weigend and Ahlrichs (def2-TZVP), and Grimme's third iteration dispersion correction (D3). Herein, this will be referred to as IEFPCM-B2PLYP-D3/def2-TZVP.

Energies are relative to structure **S4** (Figure 27) in kcal/mol from IEFPCM-B2PLYP-D3/def2-TZVP electronic energies with unscaled zero-point energy correction from IEFPCM-B2PLYP/6-31G(d)-LANL2DZ. Energies that appear in *italic text* are

Gibbs free energies (in kcal/mol) resulting from the electronic energy at IEFPCM-B2PLYP-D3/def2-TZVP level of theory with the addition of the Gibbs' free energy corrections at the B2PLYP/6-31G(d)-LANL2DZ level of the theory.

Results

Overall Reaction. In the solvent phase, the IEFPCM-B2PLYP-D3/def2-TZVP//B2PLYP/6-31G(d)-LANL2DZ (1,2-dicholorethane) model chemistry found that converting the progargylic acetate (**S1**: Figure 26) to the acetylcarene (**S2**; Figure 26) is exothermic (-26.1 kcal/mol). This is very slightly less exothermic but still very close to the value found in the gas phase (by 0.9 kcal/mol).

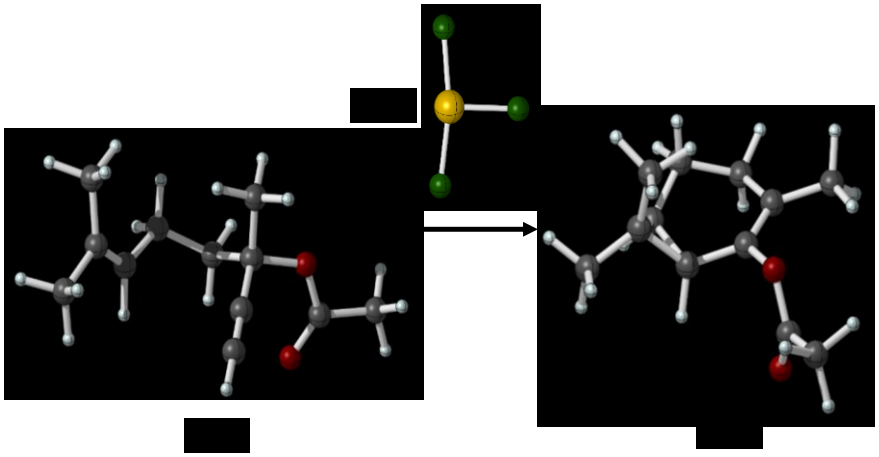

Figure 26. Solution-phase structures of the overall reaction (-26.1 kcal/mol)

Migration first pathway. As was mentioned in the previous chapter, this pathway is initiated by shifting of the acyl group. This step proceeds the same as in the gas phase with the complexation of the gold(III) chloride (**S3**; Figure 26) on the starting propargylic ester (**S1**; Figure 26). The gold complexes again from "underneath" the molecule, which activates the alkyne to be attacked by the acetoxy carbonyl oxygen. The

nucleophilic attack of the acetoxy carbonyl oxygen proceeds through a low energy barrier (**S5**; 0.7 kcal/mol) and is greatly exothermic (-25.3 kcal/mol). In the solution phase this step is much more exothermic compared to the gas-phase, which is to be expected as this step generates a cyclic oxocarbenium ion (**S6,** Figure 27). This ion is better stabilized by the addition of an implicit solvent than it is in the gas phase. The TSS for this step is the highest energy step for this pathway, which would normally indicate that it is the rate-limiting step of this pathway.

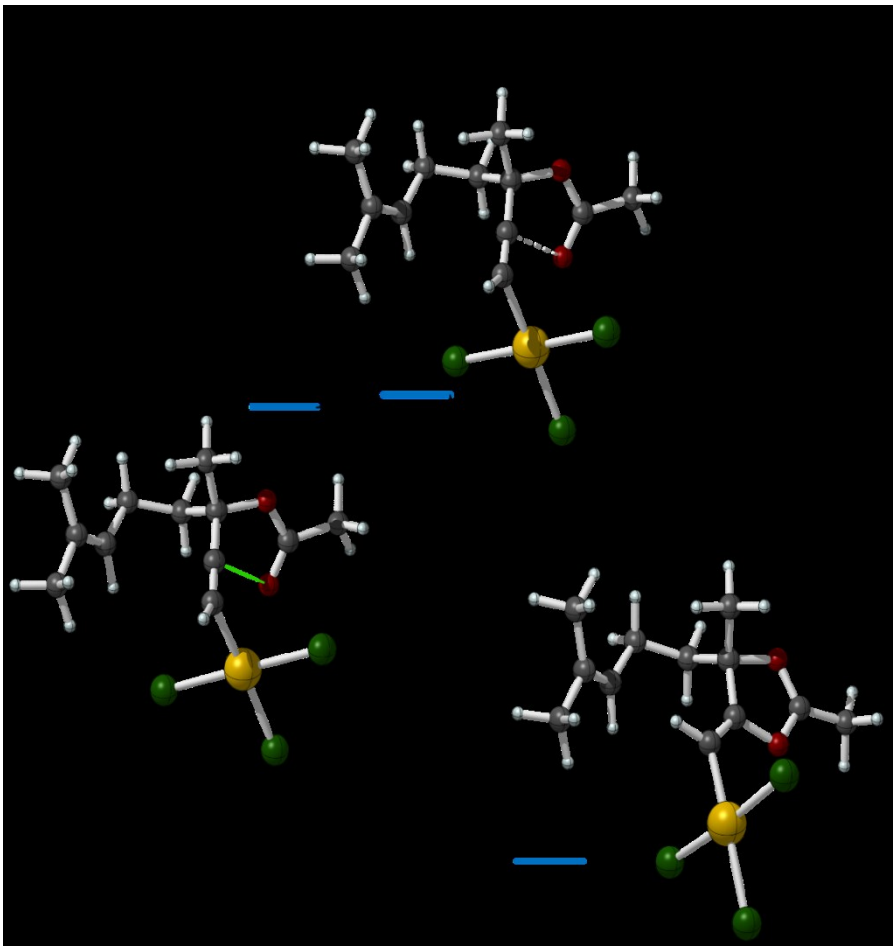

Figure 27. "Migration first" pathway showing rate-limiting step of initial acyl-group migration. Select bond distances are shown in angstroms (Å), energies shown are electronic energies with addition of zero-point correction (≈ΔH; Gibbs free energies are shown in italic) relative to **S4**

Following this formation of the cyclic oxocarbenium ion is the elimination of the adjacent oxygen, seen over **S6** to **S8** as the lengthens from 1.53Å to 3.08Å. This step is similar to the step in the gas-phase, however now it is mildly endothermic (3.0 kcal/mol) instead of exothermic (-1.6 kcal/mol; Figure 21). Breaking of the carbon-oxygen bond reforms the acetoxy carbonyl oxygen and generates an aurodiene (**S8**). At this point (as in the gas-phase pathway) chlorine on the catalyst is positioned in a way that is sterically hindering the attacking of the dimethyl alkene, so to proceed the ligand plane rotates around the dihedral Cl1-Au2-C3-C4 (See Figure 28 for numbering in blue) going from 71.5˚ to 47.7˚ (**S8** to **S10**; Figure 29). Along with this, the acetoxy group also rotates towards the terminal carbon end. The step is essentially barrierless and thermoneutral.

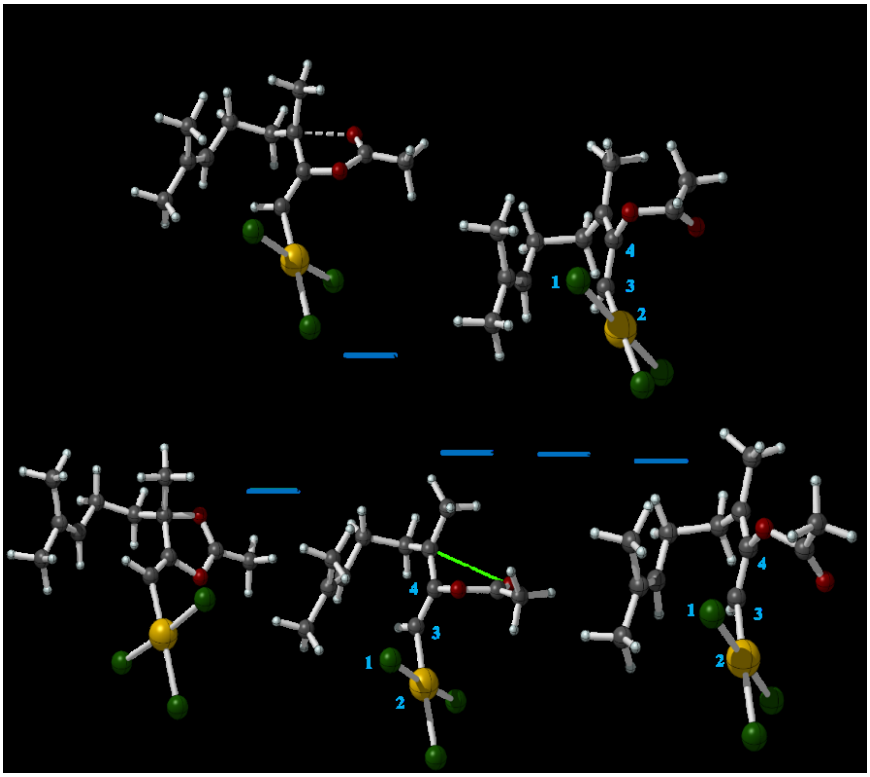

Figure 28. "Migration first" pathway showing the final acyl-migration step and conformational change with atoms numbered in blue showing indicated dihedral change. Select bond distances are shown in angstroms (Å), energies shown are electronic energies with addition of zero-point correction (≈ΔH; Gibbs free energies are shown in italic) relative to **S4**

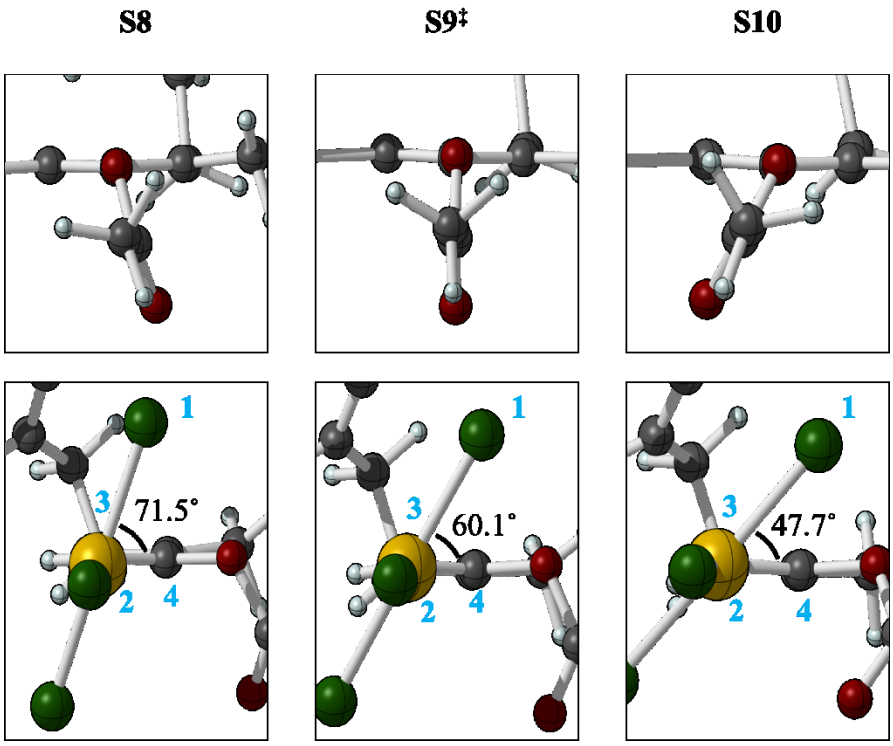

Figure 29. Side views of the two conformation changes converting **S8** to **S10**. Indicated dihedral change of ligand plane is shown in blue numbering

The cyclization step can now proceed in a similar manner to the gas phase pathways with the formation of an aurocyclobutane ring intermediate in a step-wise fashion. Electrophilic addition of the aurodiene (**S10**) onto the distal dimethyl alkene forms the 6-membered ring. In the solvent phase the chlorine on the catalyst is interacts with the 3˚ carbocation in **S12**, preventing the final ring from being formed. This step (**S10** to **S12**) is almost barrierless (0.7 kcal/mol) and exotheric (-16.1 kcal/mol). This intermediate is relatively low in energy, which may indicate it acts as a sink in this pathway. Breaking of the C-Cl interaction involves the rotation of the dihedral Cl1-Au2-C3-C4 (See Figure 30 for numbering in blue) going from 108.1˚ to 28.4˚ (**S12** to **S14**; Figure 30). This breaking of C-Cl interaction proceeds through a higher energy barrier

(14.4 kcal/mol) and the formation of the aurocyclobutane structure is endothermic (7.6 kcal/mol).

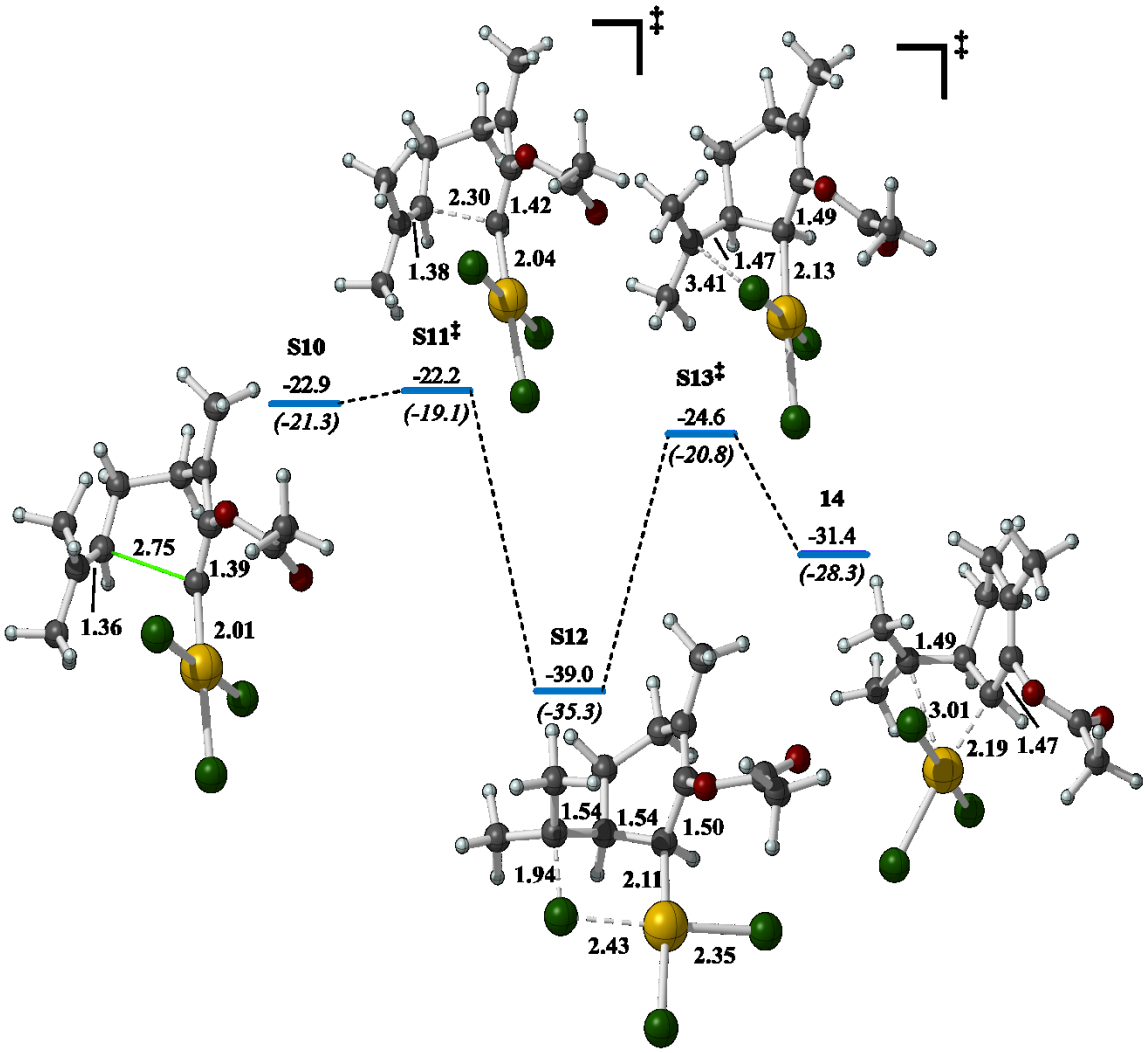

Figure 30. "Migration first" pathway of cyclization steps showing initial formation of 6 membered ring. Select bond distances are shown in angstroms (Å), energies shown are electronic energies with addition of zero-point correction (≈ΔH; Gibbs free energies are shown in italic) relative to **S4**

Reductive elimination of the catalyst proceeds through a high-energy barrier (~18.3 kcal/mol) and formation of the complexed product is endothermic (19.4 kcal/mol). One may first notice that the TSS is lower in energy than the product, and this may bring

some concern. This arises from the fact that the energies calculated are unoptimized at the level of theory they are calculated. However, at the level of theory used to optimize these structures, frequency analysis revealed then to be appropriate minima or TSSs respectively. At the higher level of theory, the true TSS should be somewhere between **S15**‡ and **S16** (Figure 31). Even with this artifact from single-point calculations, the energy barrier is very high (it is the highest single step energy barrier of this pathway).

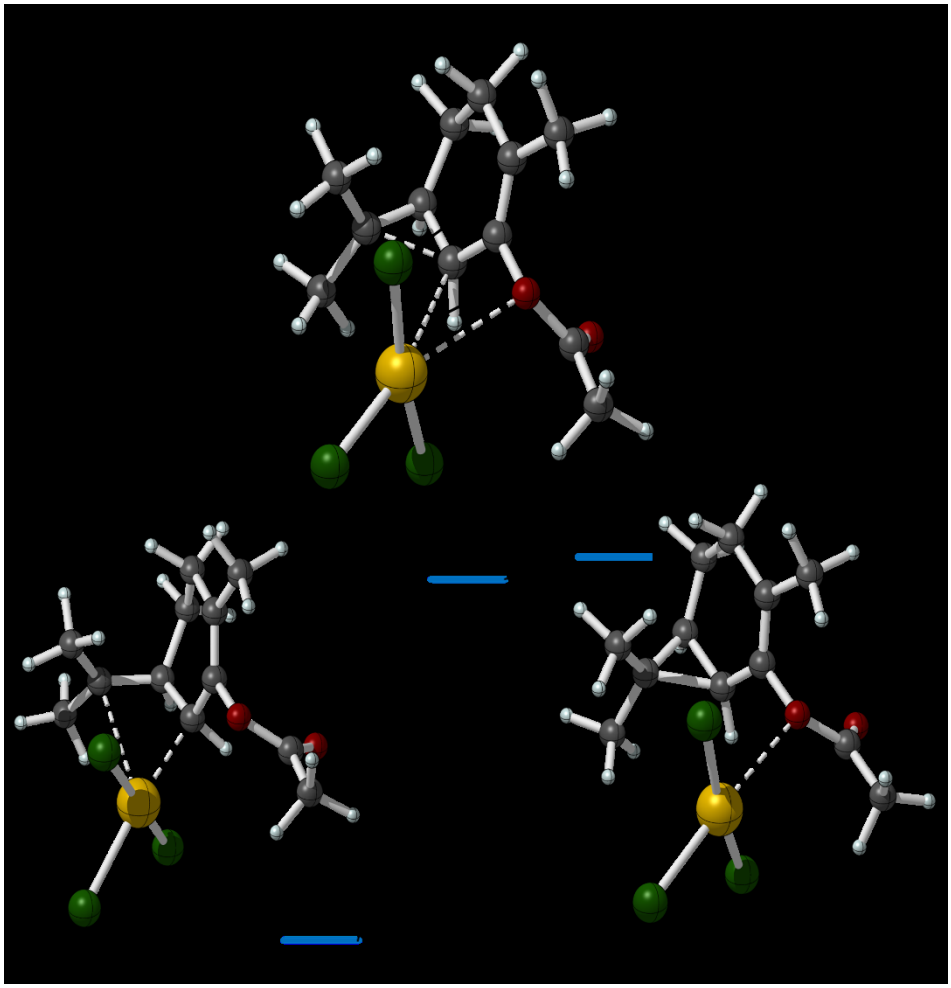

Figure 31. "Migration first" pathway showing final cyclization forming bicyclic ring structure and reductive elimination of the catalyst. Select bond distances are shown in angstroms (Å), energies shown are electronic energies with addition of zero-point correction (≈ΔH; Gibbs free energies are shown in italic) relative to **S4**

Cyclization first pathway. The initial complexation of the catalyst (**S3**) onto propargylic ester (**S1**) so that it is *anti* to the alkene tail initiates the attack and begins the cyclization step, as was seen in the gas phase pathway. Steps to locate the resulting complexed reactant did not proceed as expected. IRC calculations resulting from TSS **S18**‡ indicated the opening of the cyclized intermediate smoothly but upon many attempts to optimize this result from the IRC calculation, a cyclized structure resulted. To approximate the structure that should be found, a single point energy calculation on the analogous structure (optimized at the B2PLYP/6-31-G(d)-LANL2DZ level of theory) in the gas-phase pathway was done. Even with this approximation the complexed reactant (**S17**; Figure 32) is 4.8 kcal/mol lower in energy in this pathway compared to the complexed reactant (**S4**; Figure 27) in the previous pathway.

As in the gas-phase pathway, the cyclization step occurs in a concerted fashion, with: the formation of the six- and three-membered rings, and the catalyst sliding from the terminal end of the alkyne to the interior portion to form the cyclized intermediate as a carbene-gold complex. This step proceeds through a low energy barrier (2.7 kcal/mol) and is moderately exothermic (-19.7 kcal/mol). As in the gas phase calculation, the TSS in this step represents the highest energy barrier in the pathway, which would normally indicate the rate-limiting.

Following the cyclization step the shifting of the acyl group is initiated by the nucleophilic attack of the free carbonyl oxygen onto the carbene-gold complex (**S19**) to form the cyclic oxocarbenium ion (**S21**). This step proceeds through a mild energy barrier (**S20**‡; 6.4 kcal/mol) and is slightly exothermic (-5.4 kcal/mol). Following this step is a conformational change that was described in the gas-phase pathways. In the solvent,

however this happens in two steps (**S21** → **S23** → **S25**) instead of one step (**G19** → **G21**; Figure 25). The first step is the rotation of the ligand plane with respect to the molecule, as in the gas-phase allowing C5 to move past the chlorine. This is illustrated in Figure 33, where dihedral rotation of Cl1-Au2-C3-C4 goes from -42.8˚ (**S21**) to 2.7˚ (**S22**‡) to 37.9˚ (**S23**).

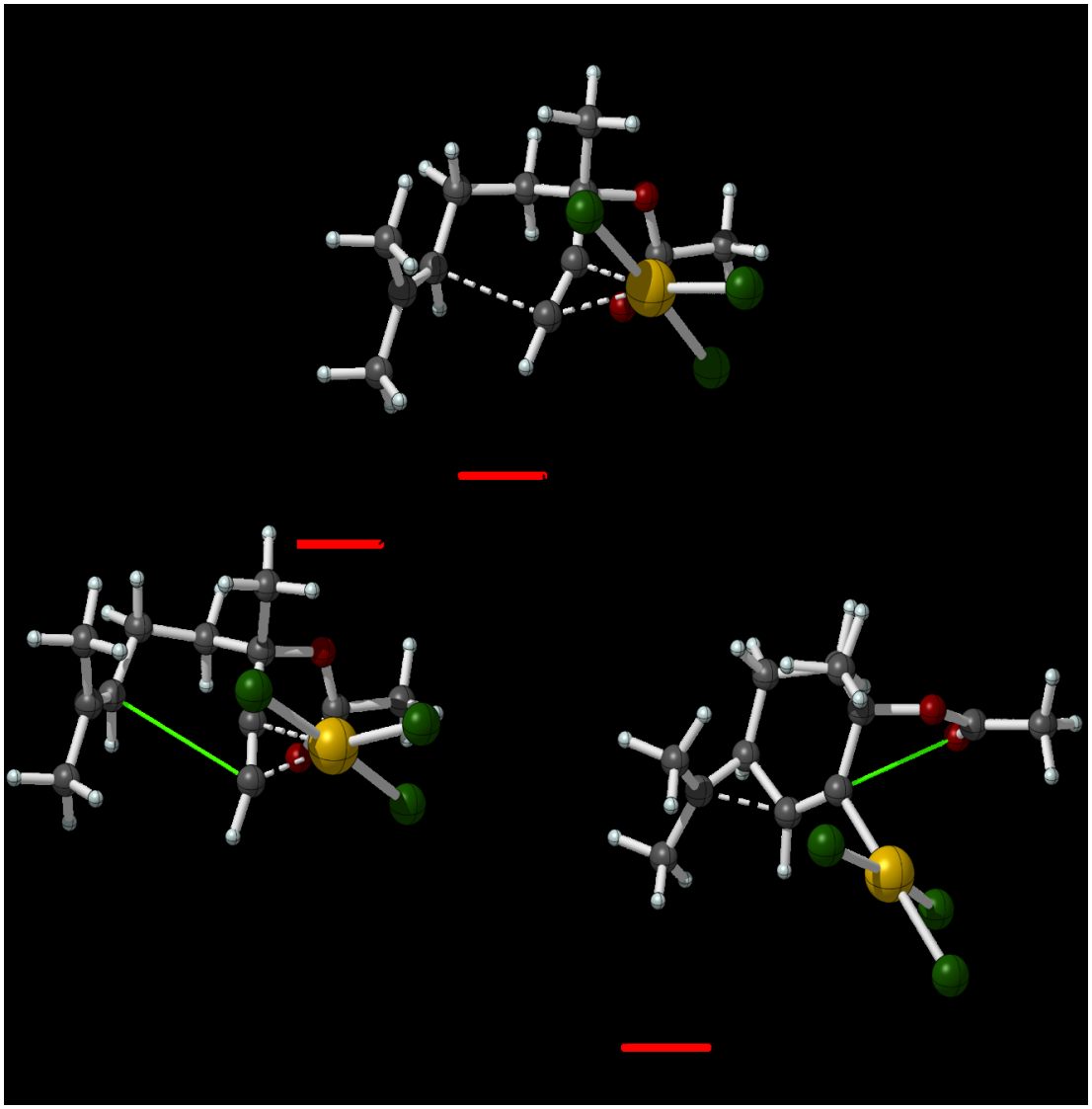

Figure 32. "Cyclization first" pathway showing formation of bicyclic ring structure. Select bond distances are shown in angstroms (Å), energies shown are electronic energies with addition of zero-point correction (≈ΔH; Gibbs free energies are shown in italic) relative to **S4**

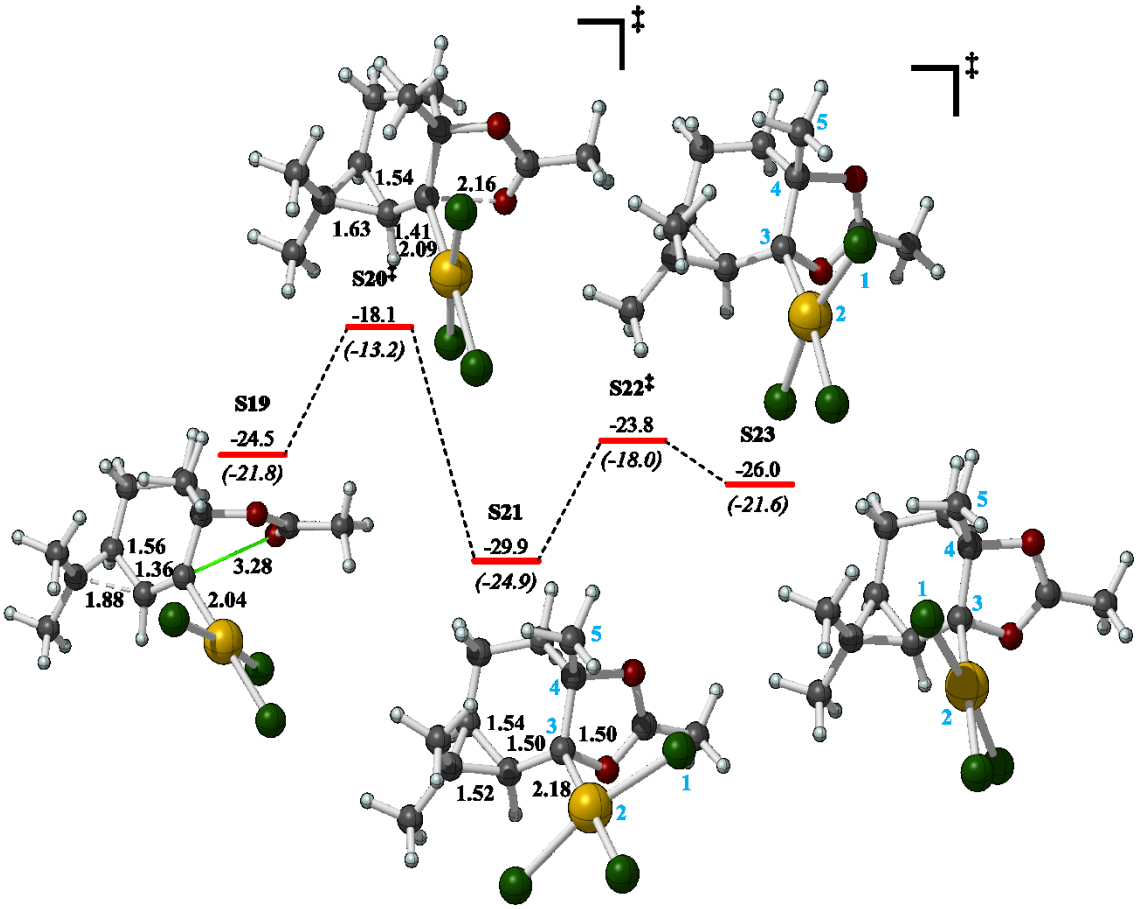

Figure 33. "Cyclization first" pathway showing initial acyl-migration and rotation of the ligand plane. Indicated dihedral change shown by numbering in blue. Select bond distances are shown in angstroms (Å), energies shown are electronic energies with addition of zero-point correction (≈ΔH; Gibbs free energies are shown in italic) relative to **S4**

The next conformational change is the gold catalyst moving to a relatively *anti*-position relative to the oxygen that will be eliminated in the next step This is illustrated in Figure 34, where dihedral rotation of Au1-C2-C3-O4 goes from 83.6˚ (**S23**) to 116.0˚ (**S24**‡) to 144.8˚ (**S25**) but is not able to move fully *anti*-to the oxygen due to the interaction between C5 and catalyst. Now with the catalyst in a nearly *anti*-position (**S25**) to the oxygen, the carbon-oxygen bond breaks restoring the carbonyl oxygen π-bond

again (**S27**). The gold complexes with the newly formed double bond, as seen in the gas phase path.

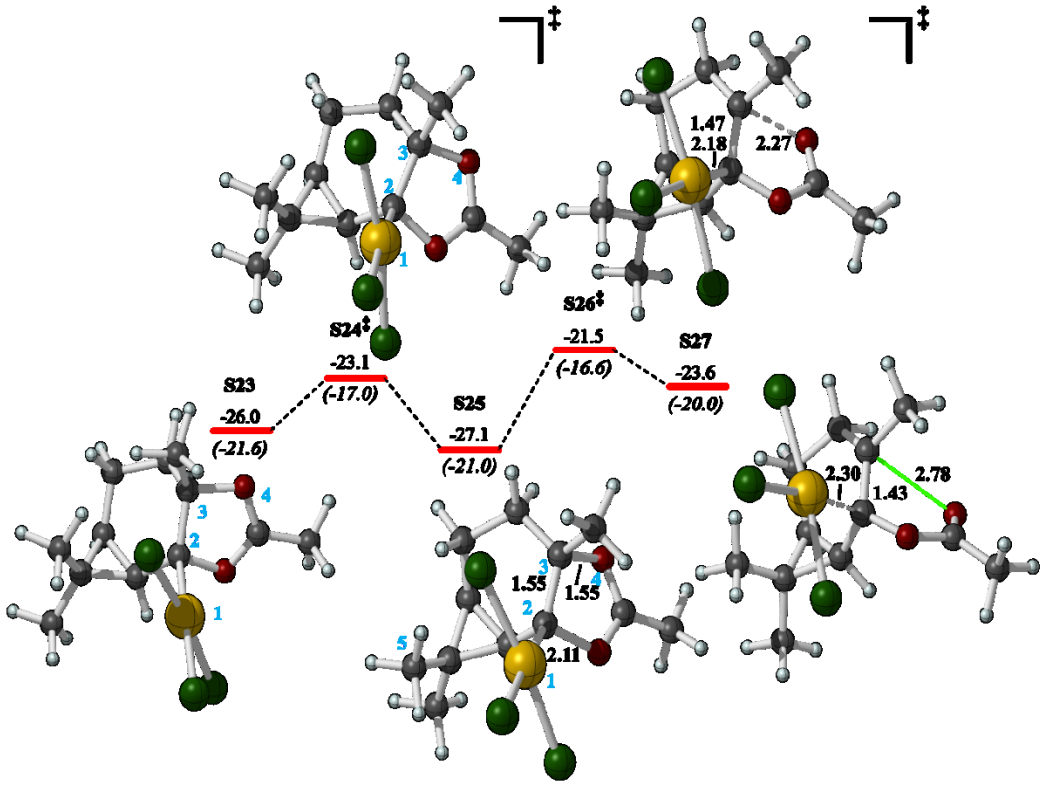

Figure 34. "Cyclization first" pathway, showing final step in acyl-migration. Indicated dihedral of conformational change shown in blue numbering. Select bond distances are shown in angstroms (Å), energies shown are electronic energies with addition of zero-point correction (≈ΔH; Gibbs free energies are shown in italic) relative to **S4**

Conclusion

Solvent-phase structures and energies for both "cyclization first" and "migration first" pathways have been presented in this chapter at the IEFPCM-B2PLYP-D3/def2-TZVP//B2PLYP/6-31G(d)-LANL2DZ (1,2-dicholorethane) level of theory. As in the gas-phase, both pathways feature multiple steps with low to moderate energy barriers.

The highest energy TSS is the initial nucleophilic attack in either pathway, which are close in energy ($\Delta H < 2.8$ kcal/mol). So, what does this mean for the preference of one pathway over the other? Chemists typically infer that the pathway with the lower energy barrier will be the preferred pathway, but as is seen in these results, there is not a meaningful energetic difference. In a catalytic cycle, once the rearrangement has completed, the catalyst restarts a new cycle. In the next chapter we will consider the cyclic nature of a catalytic cycle to help distinguish a preference for one pathway over the other.

CONCLUSION

Structures and energies for both cyclization first and migration first pathways for both gas-phase and solvent phase have been presented. In all cases the pathways feature multi-step rearrangements with low to moderate energy barriers. The solvent-phase calculations are the most closely representative of the experimental conditions so we will consider that pathway for this discussion. The highest energy TSS in both pathways is the initial attack of the nucleophile on the alkyne. These structures are very close in energy ($\Delta\Delta E^{\ddagger}$ = 2.8 kcal/mol). We investigated these TSS further with various methods (Table 5.1) to determine whether the small difference in energy is an artifact of the chosen model chemistry or if it persists indicating reality. Along with the methods used in elucidating these pathways (B3LYP, B2PLYP using both 6-31G(d)-LANL2DZ and def2-TZVP), the 2006 Minnesota functional from Truhlar's group was used (M06).[33] Corrections for dispersion (D3)[35] were also tested as the functional B3LYP has issues with describing this phenomenon.[28,29] An additional solvent model to the one shown in this work (IEFPCM) was used that was developed to provide accurate free energy of solvation (SMD).[43]

Interestingly, B3LYP shows an inversion of preference of TSSs compared to the other methods (B2PLYP and M06) with both the small [6-31G(d)-LANL2DZ] and large basis set (def2-TZVP); B2PLYP, with the small basis set, also shows this trend.

Table 1. Difference in energy (**5**‡ - **18**‡) for Rate-limiting TSSs with various model chemistries. Energies are electronic energy with either zero-point correction added or Gibbs free energy correction added in, both in kcal/mol. [a]IEFPCM solvent model, no dispersion. [b]IEFPCM solvent model, with dispersion. [c]SMD solvent model, no dispersion. [d]SMD solvent model with dispersion.

Model Chemistry		ΔE	ΔG
B3LYP/6-31G(d)-LANL2DZ	a	-1.8	-2.3
B3LYP/def2-TZVP	a	-1.3	-2.8
B2PLYP/6-31G(d)-LANL2DZ	a	-0.9	-1.2
B2PLYP/def2-TAVP//B2PLYP/6-31G(d)-LANL2DZ	a	1.6	1.3
M06/def2-TZVP	a	0.7	0.1
B2PLYP-D3/def2-TZVP//B2PLYP/6-31G(d)-LANL2DZ	b	2.8	2.5
M06-D2/def2-TZVP	b	0.7	0.1
B2PLYP/6-31G(d)-LANL2DZ (SMD)	c	0.4	0.2
B2PLYP/def2-TAVP//B2PLYP/6-31G(d)-LANL2DZ (SMD)	c	2.5	2.3
M06/def2-TZVP (SMD)	c	1.2	0.9
B2PLYP-D3/def2-TAVP//B2PLYP/6-31G(d)-LANL2DZ (SMD)	d	3.5	3.3
M06-D3/def2-TZVP (SMD)	d	1.4	1.3

With those methods that do not include dispersion correction, but use IEFPCM, the M06 functional with the large basis set shows agreement with the B2PLYP/def2TZVP single point, despite this being an unoptimized single point energy. Upon inclusion of dispersion corrections, the B2PLYP-D3 single point energy shows an

increased preference of structure **5**‡, where the M06-D3 results show very little change. The large difference observed with the B2PLYP-D3 energy due to the fact it is a single-point energy calculation on an unoptimized structure. Even with this slight error the energies are in agreement ($\Delta E < \sim 2.0$ kcal/mol). The SMD solvent model also shows a preference for structure **5**‡, both with and without dispersion corrections. Again, the B2PLYP functional single point calculation includes some error attributable to the approximation made to do a single point calculation making its preference for **5**‡ larger than the M06 functional. These results show that even with changes to the density functional the TSSs (**5**‡ and **18**‡) are very close in energy. B2PLYP and M06 both agree, while B3PLYP shows inversion of preference for **5**‡with repect to **18**‡.

Looking at the energy profiles overlaid (Figure 35) there is no clear preference between the pathways. This is a catalyzed rearrangement, meaning that once the rearrangement is done, the catalyst is regenerated and can begin the cycle again. With this we need a way to consider the circular nature of this catalytic cycle. Ideally one would translate this energetic data to something that would be good at describing a catalytic cycle, such as turnover frequency (TOF), would be useful. TOF is defined as the number of cycles per the concentration of the catalyst per time, basically how fast the catalyst can react with a substrate. Preference for one pathway of a given reaction can manifest as a substantial difference in TOF.

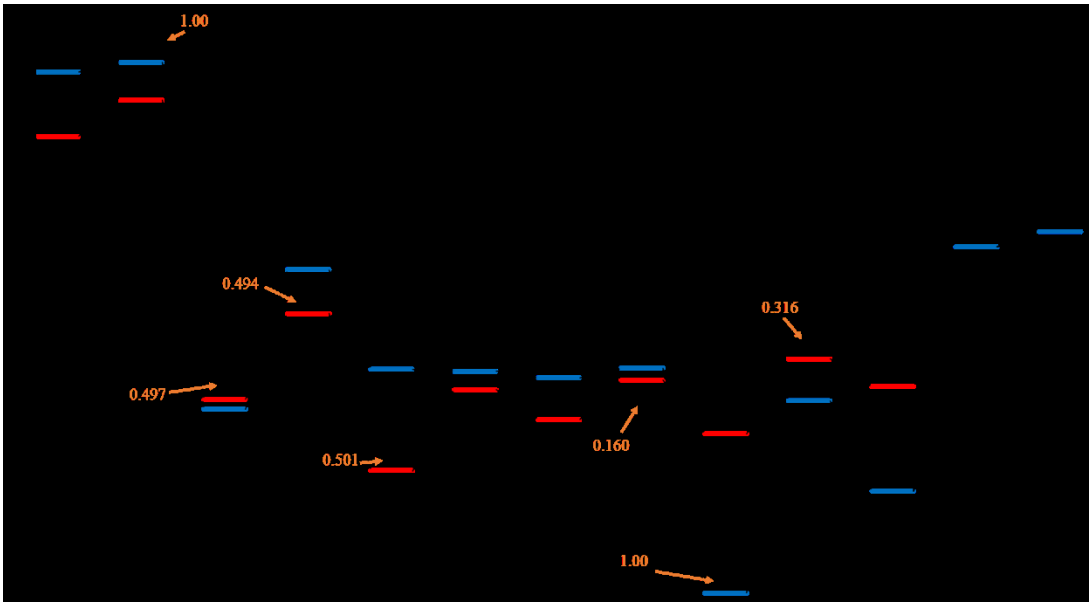

Figure 35. Overlaid energy diagrams. Red pathway – "cyclization first". Blue pathway – "Migration first". Degree of TOF control (X_{TOF}) in orange

Kozuch and Shaik[44] published a method calculate the TOF for catalytic cycles based on energetic data. Accurate and absolute TOF are, at the moment, computational impossible, but relative TOFs are tractable. Using Eyring's equation (Equation 14) from transition state theory one can establish a bridge between rate constants and Gibbs free energy.

$$k = \kappa \frac{k_B T}{h} e^{-\Delta G^{\ddagger}/RT}$$

Equation 14. Eyring's equation for relating reaction rate constant to Gibbs free energy. Transmission coefficient (κ), Boltzmann constant (k_B), temperature (T), Planck's constant (h) and the difference of Gibbs free energy between transition and intermediate ($\Delta G^{\ddagger}$)

Applying this equation to the work done by Christiansen leads to an similar and effective method of relating calculated Gibbs free energy to TOF (Equation 15).

$$TOF = \frac{k_B T}{h} \frac{e^{-\Delta G_r/RT} - 1}{\sum_{i,j=1}^{N} e^{(T_i - I_j - \delta G_{i,j})/RT}}$$

$$\delta G_{i,j} = \begin{cases} \Delta G_r \; if \; i > j \\ 0 \; if \; i \leq j \end{cases}$$

Equation 15. Turn over frequency equation calculated from Gibbs free energy of intermediates (I_j) and transition states (T_i). $\delta G_{i,j}$ this is the Gibbs free energy of the reaction when the transition state (i) occurs after the intermediate (j) in the forward direction of the reaction.

Applying this equation to the work done here we find that the "cyclization first" pathway is 630 times faster than the "migration first" pathway. This suggests that the cyclization first pathway is the dominate pathway of the rearrangement. What makes this pathway preferred even when the "rate-limiting" step in each is very close in energy? Using the methods described by Kozach and Shaik, one can look into what effect each structure has on the TOF, this is termed the degree of TOF control (X_{TOF}; Equation 16). X_{TOF} is normalized so a number closer to 1 represents a structure that has larger impact on the TOF.

$$X_{TOF}, T_i = \frac{\sum_j e^{(T_i - I_j \delta G_{i,j})/RT}}{\sum_{ij} e^{(T_i - I_j \delta G_{i,j})/RT}}$$

$$X_{TOF}, I_j = \frac{\sum_i e^{(T_i - I_j \delta G_{i,j})/RT}}{\sum_{ij} e^{(T_i - I_j \delta G_{i,j})/RT}}$$

Equation 16. Equations for determining degree of TOF (X_{TOF}) control for transition states (T_i) and intermediates (I_j)

Structures with significant X_{TOF} are TOF-determining transition states (TDTSs) or TOF-determining intermediates (TDIs). For the "migration first" pathway the TDTS and TDI are what one would expect when looking at the energy diagram. The TDTS is **5**‡ with an X_{TOF} of 1.00 and the TDI is **12** with an X_{TOF} of 1.00. This is expected as these were the highest and lowest points on the potential energy diagram. The TDTS is the step responsible for the initial attack starting the migration of the acyl group. The TDI is the structure in which the chlorine ligand is interacting with tertiary carbocation during the cyclization step. For the "cyclization first" pathway things are much different. The highest energy TSS is not a TDTS in fact the distinction of TDTS is shared by three different transition states, **20**‡ (X_{TOF} = 0.494), **24**‡ (X_{TOF}=0.160), and **26**‡ (X_{TOF} = 0.316). The distinction of TDI is shared by two intermediates **19** (TOF = 0.497) and **21** (X_{TOF}= 0.501). The TDTSs are the steps responsible for migration of the acyl group.

This shows that the extremes on the potential energy diagram may not always be the TDTS or TDI due the cyclic nature of the forward flowing catalytic cycle. Knowing what structures contribute the greatest effect on the TOF can also help in planning a way to improve the TOF. If the TDTS is stabilized then the TOF can be improved. Destabilization of the TDI, raising the energy floor, will also lead to improvement of the TOF as the catalytic sinks will be shallower.

This model is not without its approximations. The first is that the Gibbs free energies used in these equations need to be accurate. Accurate Gibbs energies are much harder to calculate than electronic energies. On a related note, one must choose a solvent model that will provide accurate Gibbs energies, however, when comparing relative TOF of systems containing the same molecularity error from this source will be minimized.

Another approximation is that the reaction is at steady state and is not showing chaotic behavior. This is a reasonable approximation when the reaction takes place in a solvent as the intermediates can quickly relax. This last part assumes that the intermediates do quickly relax and redistribute the kinetic energy. Perhaps this rearrangement does not conform to the minimum energy pathway and the kinetic energy should not be neglected. If the kinetic energy term was included, the rearrangement may behave differently. This leads to the future of this project: using the methods here as a starting point to begin molecular dynamic simulations that will include molecular motion as a function of time. This project will start simulations with the catalyst complexing to the catalyst. Test runs have been conducted and they have successfully shown the formation of a carbon-oxygen bond initiating the “migration first” pathway.

REFERENCES

1. Bernstien, P.; *The Power of Gold The history of an Obsession.* John Wiley & Sons. Ltd: Chichester, England, **2004**.

2. Thayer, J.; In *Relativistic Methods for Chemists.* Barysz, M., Ishikawa, Y. *Challenges and Advances in Computational Chemistry and Physics.* Springer Netherlands, **2010**; Vol 10.

3. Bartlett, N.; Gold Bulletin, **1998**, 31 22-25.

4. Toste, D., Michelet, V.;*Gold Catalysis An Homogenous Approach.* Catalytic Science Series; Imperial College Press: Covent Garden, London, **2014**.

5. Ito*, Y.*, Sawamura, M. and Hayshi, T.; *J. Am. Chem. Soc*., **1986**, 108, 6405-6406.

6. *Dewar, M. J. S.; Soc. Chim. Fr*., **1951**, 19, 71-79.

7. *Chatt, J.* and Duncanson, L. A.; *J. Chem. Soc.,* **1953**, 0, 2939-2947.

8. Teles, J. H., Brode, S.; *Angew. Chem., Int. Ed*. **1998**, 37, 1415-1418.

9. Mizushima, E., Sato, K., Hayshi, T., Tanaka, M.; *Angew. Chem., Int. Ed*. **2002**, 41, 4563-4565.

10. Leyva, A. and Corma, A.; *J. Org. Chem.*, **2009**, 74, 2067-2074.

11. Fuckuda, Y. and Utomoto, K.; *J. Org. Chem.,* **1991**, 56, 3729-3731.

12. Aponick, A., Li, C.-Y., Malinge, J., Marques, E. F.; *Org. Lett.,* **2009**, 11, 4624-4627.

13. Blanc, A., Alix, A., Weibel, J.-M., Pale, P.; J. *Org. Chem.,* **2009**, 74, 5342-5348.

14. Belting, V., Krause, N.; *Chem*., **2009**, 7, 1221-1225.

15. Strickler, H., Davis, J. B., Ohloff, G.*; Helv. Chim. Acta*, **1976**, 59, 1328-1332.

16. Rautenstrauch, V.; *J. Org. Chem*. **1984**, 49, 950-952

17. Mainetti, E., Mouries, V., Fensterbank, L., Malacria, M. and Marco-Contelles, J.; *Angew. Chem. Int. Ed.,* **2002**, 41, 2132-2135.

18. de Boer, T. J., Backer, H.; *J. Org. Synth*. **1956**, 36, 16.

19. Furstner, A., Hannen, P.; *Chem. Eur. J.,* **2006**, 12, 3006-3019.

20. Velazco, M., Wuensche,. Deladoey, P.; Use of cubebol as a flavoring ingredient. US 6214788 B1, Mar 28, **2000**.

21. Smith, J.; *Organic Chemistry,* 2nd ed ;McGraw-Hill: New York, NY, 2008

22. Grossman, R.; *The Art of Writing Reasonable Organic Reaction.Mechanisms*. 2nd ed. Springer Science+Business Media, Inc.: New York, NY, **2003**.

23. Lewars, E.; *Computational Chemistry Introduction to the Theory and Applications of Molecular and Quantum Mechanics*. 2nd Ed.; Springer Science+Business Media, Inc.: New York, NY, **2011**.

24. Cramer, C.; *Essentials of Computational Chemsitry Theories and Models*. 2nd Ed.:John Wiley & Sons Ltd: Chichester, England, **2004**

25. Becke, A. D.; J. Chem. Phys., **1993**, 98, 5648-5652.

26. Becke, A. D. Phys. Rev. A., **1988**, 38, 3098-3100.

27. Lee, C., Yang, W., Parr, R. G.; Phys Rev. 1988, 37, 785-789

28. Wodrich, M. D.; Org. Lett., 2006, 8, 3631-3634.

29. McKee, Mw. C., Schelyer, P.; J. Am. Chem. Soc., **2013**, 135, 13008-13014.

30. Tsuzuki, S., Lüthi, H. P.; J. Chem. Phys., **2001**, 114, 3949-3957.

31. Zhao, Y., Truhlar, D. G.; J. Phys. Chem. A. **2006**, 110, 10478-10486.

32. Grimme, S. J. Chem. Phys., **2006**, 124, 034108.

33. Zhao, Y., Truhlar, D.; Theor. Chem. Acc., **2008**, 120, 215-241.

34. Liptrot, D., Power, P.; Nature Rev. Chem., **2017**, 1.

35. Grimme, S., Antony, J., Ehrlich, S., Krieg, H.; J. Chem. Phys., **2010**, 132, 154104.

36. Kang, R., Chen, H., Shaik, S., Yao, J.; J. Chem. Theory Comput., **2011**, 7, 4002-4011.

37. Ciancaleoni, G., Rampino, S., Zuccaccia, D., Tarantelli, F., Belanzoni, P., Belpassi, L.; J. Chem. Theory. Comput. **2014**, 10, 1021-1034.

38. Hay, P. J., Wadt, W. R.; J. Chem. Phys, **1985**, 82, 270-283.

39. Hay, P. J., Wadt, W. R.; J. Chem. Phys, **1985**, 82, 299-310.

40. Frisch, M. J.; Trucks, G. W.; Schlegel, H. B.; Scuseria, G. E.; Robb, M. A.; Cheeseman, J. R.; Scalmani, G.; Barone, V.; Mennucci, B.; Petersson, G. A.; Nakatsuji, H.; Caricato, M.; Li, X.; Hratchian, H. P.; Izmaylov, A. F.; Bloino, J.; Zheng, G.; Sonnenberg, J. L.; Hada, M.; Ehara, M.; Toyota, K.; Fukuda, R.; Hasegawa, J.; Ishida, M.; Nakajima, T.; Honda, Y.; Kitao, O.; Nakai, H.; Vreven, T.; Montgomery Jr., J. A.; Peralta, J. E.; Ogliaro, F. o.; Bearpark, M. J.; Heyd, J.; Brothers, E. N.; Kudin, K. N.; Staroverov, V. N.; Kobayashi, R.; Normand, J.; Raghavachari, K.; Rendell, A. P.; Burant, J. C.; Iyengar, S. S.; Tomasi, J.; Cossi, M.; Rega, N.; Millam, N. J.; Klene, M.; Knox, J. E.; Cross, J. B.; Bakken, V.; Adamo, C.; Jaramillo, J.; Gomperts, R.; Stratmann, R. E.; Yazyev, O.; Austin, A. J.; Cammi, R.; Pomelli, C.; Ochterski, J. W.; Martin, R. L.; Morokuma, K.; Zakrzewski, V. G.; Voth, G. A.; Salvador, P.; Dannenberg, J. J.; Dapprich, S.; Daniels, A. D.; Farkas, Ã. d. n.; Foresman, J. B.; Ortiz, J. V.; Cioslowski, J.; Fox, D. J. Gaussian 09, Revision D.01; Gaussian, Inc.: Wallingford, CT, USA, **2009**.

41. Weigen, F., Phys. Chem. Chem. Phys., **2006**, 8, 1057-1065.

42. Miertus, S., Scrocco, E., Tomasi, J. Chem. Phys, **1981**, 55, 117-129.

43. Marenich, A. V., Cramer, C. J., Truhlar, D. G.; J. Phys. Chem., **2009**, 113, 6378-6396

44. Kozuch, S., Shaik, S., Acc. Chem. Res. **2011**, 44, 101-110.